Monthly Notices of the ROYAL ASTRONOMICAL SOCIETY

MNRAS **508,** 1870–1887 (2021) https://doi.org/10.1093/mnras/stab2709
Advance Access publication 2021 September 21

AutoProf – I. An automated non-parametric light profile pipeline for modern galaxy surveys

Connor J. Stone [1]★ Nikhil Arora [1] Stéphane Courteau [1] and Jean-Charles Cuillandre [2]

[1]*Department of Physics, Engineering Physics & Astronomy, Queen's University, Kingston, ON K7L 3N6, Canada*
[2]*AIM, CEA, CNRS, Université Paris-Saclay, Université de Paris, F-91191 Gif-sur-Yvette, France*

Accepted 2021 September 15. Received 2021 September 15; in original form 2021 June 24

ABSTRACT

We present an automated non-parametric light profile extraction pipeline called AUTOPROF. All steps for extracting surface brightness (SB) profiles are included in AUTOPROF, allowing streamlined analyses of galaxy images. AUTOPROF improves upon previous non-parametric ellipse fitting implementations with fit-stabilization procedures adapted from machine learning techniques. Additional advanced analysis methods are included in the flexible pipeline for the extraction of alternative brightness profiles (along radial or axial slices), smooth axisymmetric models, and the implementation of decision trees for arbitrarily complex pipelines. Detailed comparisons with widely used photometry algorithms (PHOTUTILS, XVISTA, and GALFIT) are also presented. These comparisons rely on a large collection of late-type galaxy images from the PROBES catalogue. The direct comparison of SB profiles shows that AUTOPROF can reliably extract fainter isophotes than other methods on the same images, typically by >2 mag arcsec^{-2}. Contrasting non-parametric elliptical isophote fitting with simple parametric models also shows that two-component fits (e.g. Sérsic plus exponential) are insufficient to describe late-type galaxies with high fidelity. It is established that elliptical isophote fitting, and in particular AUTOPROF, is ideally suited for a broad range of automated isophotal analysis tasks. AUTOPROF is freely available to the community at: https://github.com/ConnorStoneAstro/AutoProf.

Key words: methods: data analysis – techniques: image processing – techniques: photometric – galaxies: general – galaxies: photometry.

1 INTRODUCTION

Images of galaxies contain a wealth of valuable information about their structure, stellar populations, dust content, dynamics, and evolutionary history. A common approach to extract this information from galaxy images involves modelling structural components, such as a bulge, disc, bar, and spiral arms, with pre-determined fitting functions (Hubble 1930; de Vaucouleurs 1948; Einasto 1965; Sérsic 1968; Freeman 1970). While these model decompositions can be arbitrarily complex (Kent 1985; Peng et al. 2002, 2010; Erwin 2015), their execution may be time consuming and require individual attention. Parametric models typically struggle with complex galaxy morphologies and manual intervention is necessary to return realistic solutions. In practice, large galaxy surveys typically employ simplified models that can be automated (e.g. Kelvin et al. 2010; Simard et al. 2011).

A complimentary approach to analysing galaxy images involves their non-parametric[1] representation into elliptical isophotes [contours of constant surface brightness (SB)] yielding average brightness profiles for each galaxy. Much like the parametric methods above, the non-parametric modelling of elliptical isophotes from galaxy images has a rich history (e.g. Carter 1978; Kent 1983; Davis et al. 1985; Lauer 1985; Tody 1986; Jedrzejewski 1987).

The extraction of representative azimuthally averaged profiles of SB, position angle (PA), and ellipticity as a function of (galactocentric) radius takes advantage of the near axisymmetry of a 2D image of a galaxy, which is a projection on the sky of a complex 3D object. Non-parametric reductions of galaxy images into 1D SB profiles can then be further decomposed into structural parameters (MacArthur, Courteau & Holtzman 2003; Ciambur 2016; Bottrell et al. 2017; Gilhuly & Courteau 2018).

Non-parametric models and complete pipeline automation in the era of large galaxy surveys (e.g. Amiaux et al. 2012; Ivezić et al. 2019; Mosby et al. 2020) will allow extensive representations of the data complexity available in such surveys. However, current techniques of extracting robust non-parametric light profiles can still be time consuming and require human intervention. For instance, Smith et al. (2021) estimated a time period of 2 yr to extract light profiles interactively for 10^5 objects. A fast, flexible, automated tool to extract such galaxy light profiles will be required to take full advantage of the influx of photometric survey data in the next decade and beyond.

In this paper, we present a package called AUTOPROF, for the fast, automated, non-parametric extraction of SB profiles using elliptical isophotes. AUTOPROF borrows from Jedrzejewski (1987, hereafter J87), though with the addition of regularization techniques

★ E-mail: connor.stone@queensu.ca

[1]A 'non-parametric' isophotal fit can use many parameters to describe the PA, ellipticity, and semimajor axis of each elliptical isophote, however these parameters have a non-trivial mapping to a structural model such as a bulge, disc, bar, etc.

from machine learning, and yields robust SB profiles that match light distributions, even in complex systems. It requires no human intervention and can process a galaxy image in ∼15 s (on a single 4GHz Intel i7-4790K processor core), though processing time varies quadratically with the galaxy size (in this case, ∼700 pixels). AUTOPROF is a pipeline building code designed to take full advantage of modern galaxy surveys which allows arbitrarily complex analysis for advanced users, yet offers a robust default setup for rapid startup. We compare AUTOPROF to a number of established photometry codes using DESI Legacy Sky Survey images (Dey et al. 2019) to demonstrate the context in which AUTOPROF is ideally suited.

The format of the paper is as follows. Section 2 reviews the default AUTOPROF pipeline, with steps such as background, point-spread-function (PSF) estimations, centroid algorithm, isophotal fitting, light profile extraction, fit checks, and forced photometry. AUTOPROF offers a suite of advanced pipeline tools presented in Section 3, such as star masking, wedge-sector radial sampling, lateral slicing, smooth model image reconstruction, as well as instructions to integrate and execute new functions. Section 4 offers comparisons of AUTOPROF output products with those from similar isophotal fitting codes, such as (i) the 'PHOTUTILS' implementation of the non-parametric isophotal fitting algorithm by J87, (ii) the PROFILE algorithm (Lauer 1985; Courteau 1996) within the XVISTA software package for astronomical image processing,[2] and (iii) the parametric galaxy image modeller GALFIT (Peng et al. 2010) which decomposes galaxy images using pre-defined parametric models. These comparisons highlight the pros and cons of model-independent and parametric light profile extractions, and our ability to scale these operations to very large multiwavelength photometric investigations. Main results and typical applications for AUTOPROF are summarized in Section 5. AUTOPROF is provided to the community in a flexible and modular software package. Step-by-step instructions to run AUTOPROF can be found in the documentation of the code repository: https://github.com/ConnorStoneAstro/AutoProf.

2 THE DEFAULT AUTOPROF PIPELINE

AUTOPROF is an automated, fully featured, light profile extraction pipeline with modular steps. The core AUTOPROF algorithm fits elliptical isophotes automatically to galaxy images and extracts accurate flux measurements along those ellipses. The user constructs a configuration file, which specifies the images for AUTOPROF to analyse and the steps involved in that analysis. Provided a galaxy image, pixel scale, and flux zero-point, AUTOPROF can automatically determine the sky level, galaxy centre, fit elliptical isophotes, and extract an SB profile. After extraction, AUTOPROF reports on the quality of the extraction and flags potentially problematic fits (see Section 2.7); this is important in the fully automated domain it is intended for. AUTOPROF is designed to condense these and other tasks into an automated pipeline. This section presents AUTOPROF's default pipeline to analyse galaxy images.

2.1 Background estimation

All galaxy images contain a background signal level resulting from a combination of sky brightness, read noise, zodiacal light, diffraction, and a host of other effects. To ensure that a light profile contains only signal from the galaxy, this background signal must be removed. This is especially important for AUTOPROF, which is designed to push faint SB limits for a given observing campaign (often more than 4 magarcsec^{-2} deeper than the background noise level). The default background calculation uses the mode of the pixel flux values, which is less affected by outliers relative to mean or median estimates. This method uses all pixels that are within 1/5th of the image width from the edge. Large images with sufficient sky background areas will be beneficial for such calculations. The peak of a Gaussian smoothed density profile in flux space is then identified and used as the background sky level (see Fig. 1). The smoothing function is given by equation (1):

$$B = \mathrm{argmax}_x \sum_i e^{-\frac{(f_i - x)^2}{\sigma^2}} \quad (1)$$

where B is the mode background level, f_i is the flux of the i^{th} pixel, and σ is the smoothing length. The smoothing length is $\sigma = \Delta_{25}^{75}/\log_{10}(\sqrt{N})$, where Δ_{25}^{75} is the interquartile range, and N

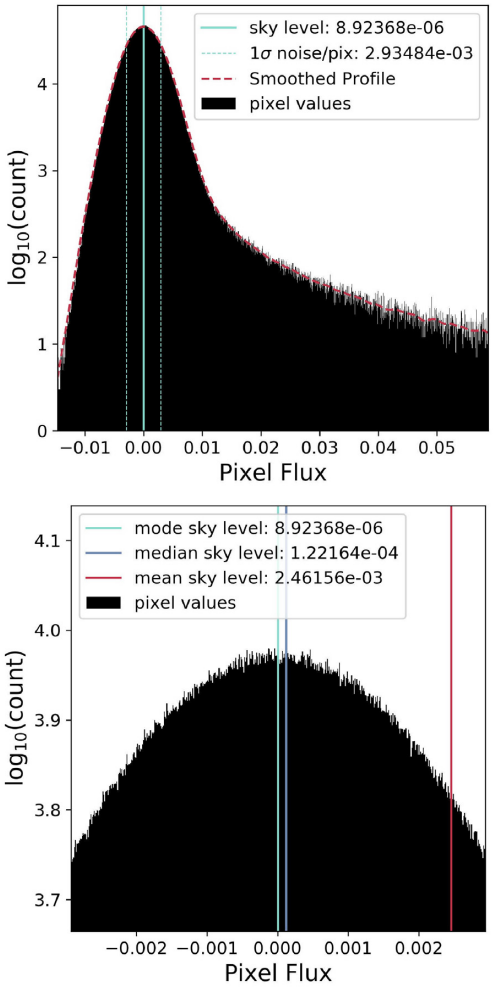

Figure 1. Background estimation procedure from the default AUTOPROF pipeline for *ESO479-G1*. Top figure: pixel flux values from the outer 1/5th border of the image (see Fig. 2). In black, a histogram of flux values, the red dashed line is a Gaussian smoothed profile, the blue vertical lines show the mode flux value and the 1σ scatter (as measured based on flux values below the mode flux). Bottom figure: zoom-in on the peak of the flux distribution. Also shown are mean and median values, both of which are biased high due to unmasked objects (stars, background galaxies, etc.).

[2]We shall refer to the PROFILE isophotal fitting software as 'XVISTA'. The XVISTA software package is maintained by Jon Holtzman at NMSU (New Mexico State University); http://ganymede.nmsu.edu/holtz/xvista/

is the number of pixels (the precise choice of smoothing length is not very important for most tasks). The use of mode averaging and interquartile ranges means that bright unwanted sources (stars, cosmic rays, and hot pixels) have minimal effect on the estimated background. Large faint sources, such as Galactic cirri, nearby galaxies, and intra-cluster light can bias the mode estimator. If these sources affect an appreciable fraction of the total number of pixels (approximately one quarter of the field of view (FOV)) then the background estimator will likely be biased high. Such areas should be avoided, masked, or a more sophisticated background estimation algorithm could be applied. The sky noise is taken as the 68.3 percentile of flux values below the sky level ($\Delta^{100}_{31.7}$). For properly processed astronomical images, free of systematic effects (poor detrending, faulty large scale background removal), flux values below the sky level should mostly be contributed by Poisson noise while flux values above the sky level can be contaminated by faint sources.

The default mode background estimation is accurate enough for most purposes, and is reliable in an automated framework. However, more precise background levels can be determined with specialized clipping procedures (Ratnatunga & Newell 1984; Akhlaghi 2019). The user may take advantage of such external techniques and provide AUTOPROF with a specified background level. AUTOPROF also includes a wrapper of the PHOTUTILS dilated source mask method, which identifies bright sources and masks sky annuli around them to remove faint tails from the image. While effective, this method is slower than the AUTOPROF default.

2.2 PSF estimation

The default PSF estimation method searches for star candidates using a peak finding convolution filter. Once selected, stellar fluxes are measured within circular apertures using a Lanczos interpolation between pixels until the flux value reaches half of the central peak value. The full width at half-maximum (FWHM) is taken as the PSF. While measuring the flux, AUTOPROF also tracks the low order fast-Fourier transform (FFT) coefficients of flux values around each star candidate. Specifically, the 'deformity' metric for perturbations from a circle are measured as:

$$d = \sum_{i=1}^{5} \left| \frac{\mathcal{F}_i}{\tilde{\mu} + \sigma_b} \right| \tag{2}$$

where d is the deformity, $\mathcal{F}_i$ is the i^{th} Fourier coefficient, $\tilde{\mu}$ is the median flux, and σ_b is the background noise per pixel (Section 2.1). Note that $\tilde{\mu} + \sigma_b$ is nearly equivalent to $\mathcal{F}_0$, though it is more stable at low S/N in the presence of outliers. Once 50 star candidates have been measured around the galaxy, a median of the 'roundest' half of the star candidates is used as the image flux value; where roundness is determined by the power in low order FFT coefficients previously measured. Fig. 2 represents the PSF estimation procedure graphically.

Since AUTOPROF samples flux values along isophotes, a PSF estimate is not required for its calculations. AUTOPROF operates on galaxies of all apparent sizes from only a few dozen to many thousand of pixels across. Primarily, the PSF estimate is used to set a meaningful scale on the image, determining the lower bound for geometrically growing radii when fitting/sampling from the image. Thus AUTOPROF is robust to imprecise PSF estimates. However, the approximate PSF of inner isophotes at or below the PSF scale will be biased round due to resolution effects.

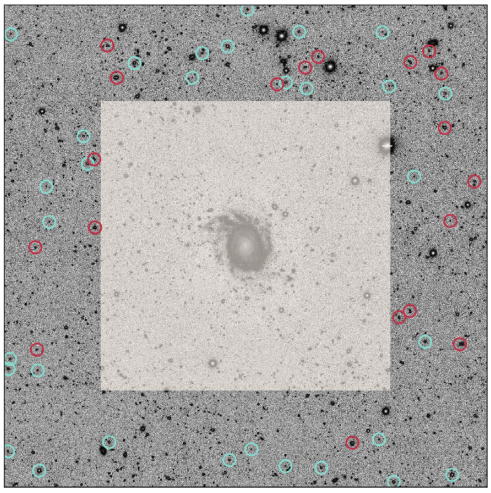

Figure 2. PSF estimation procedure from the default AUTOPROF pipeline for *ESO479-G1*. Highlighted with circles is a selection of randomly chosen star candidates from the image. In red, star candidates that have been rejected based on the roundness criteria of power in low order FFT coefficients. In blue, star candidates that have been accepted. The PSF is taken as the FWHM, determined by a Lanczos interpolation between pixels determining the diameter at which the flux reaches half the central value. The shaded area is masked from the PSF analysis; this is the same region as the background estimation (see Section 2.1).

2.3 Centre finding

The AUTOPROF default centre finding algorithm iteratively updates a candidate centre until it reaches a global flux peak. The candidate centre may be the image centre, or one supplied by the user; this allows AUTOPROF to examine any galaxy in the image. Generally, the algorithm starts searching from the centre of the image or the user may provide an initial centre to AUTOPROF in fractional pixel coordinates. From the initialization point, 10 circular apertures are created out to 10 times the PSF size and samples flux values around each aperture. An FFT is taken for the flux values around each circular aperture and the phase of $\mathcal{F}_1$ is used to determine the direction of increasing brightness. Taking the average direction, flux values are sampled along a line from the centre out to 10 times the PSF. A parabola is fit to the flux values and the centre is then updated to the maximum of the parabola. This is repeated until the updated steps move by half a PSF. To refine the centre estimate at a level below 1 pixel, a Nelder-Mead simplex optimizer is used to minimize $|\mathcal{F}_1/(\tilde{\mu} + \sigma_b)|$ evaluated on three circular apertures (out to three PSF). Fig. 3 illustrates the iterative centre finding procedure. In the figure, we intentionally initialize the algorithm away from the galaxy centre; the path demonstrates how the centre finding method can ignore local features to fit the global centre of the galaxy. This method of centre finding is accurate when initialized in the main part of a galaxy, and works well for objects that are roughly centred on the image plane. Failed centre identification is discussed in Section 2.7.

2.4 Initialization

The Fourier analysis that determines the initial isophotal parameters fits the global PA and ellipticity of each ellipse in a two-step process. First, a series of circular apertures are sampled geometrically in radius starting at the centre until they approach the background level of the image. An FFT is taken for the flux values around each circular aperture and the phase of $\mathcal{F}_2$ is used to determine a direction.

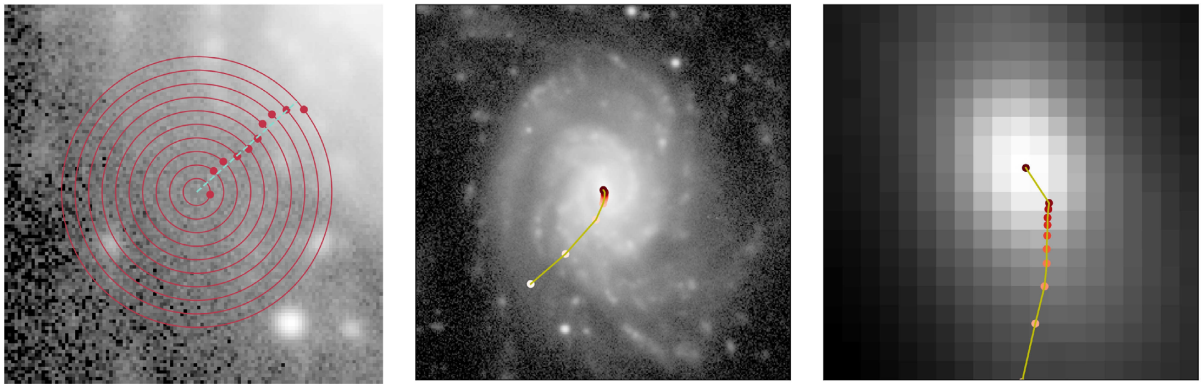

Figure 3. Centre finding procedure from the default AUTOPROF pipeline for *ESO479-G1*. Left: a single iteration of the centre finding procedure, 10 rings of flux are extracted (red rings) and the phase of $\mathcal{F}_1$ is used to provide a direction of increasing flux (red dots on the rings). The 10 directions are then averaged to choose a robust direction of increasing flux (blue dashed line direction) and a parabola is fit along that direction to determine the location of the maximum (blue dashed line length). Middle: the path taken by the iterative centre finding method. The first few steps are as large as is allowed (to the edge of the 10th ring), then smaller steps refine the centre. Right: a zoom-in at the centre of the galaxy showing the final few steps. The large last step shows the result of the centre refining with only three flux rings instead of the 10 used for the global fit; this smaller window can only be used near the global maximum as it can easily be caught in local maxima.

The average direction for the outer isophotes is taken as the PA of the galaxy. Secondly, with fixed PA, the ellipticity is optimized to minimize $|\mathcal{F}_2/(\tilde{\mu}+\sigma_b)|$. Fig. 4 illustrates the two-step process of fitting the global PA and ellipticity.

The errors on PA and ellipticity are assessed by fitting multiple isophotes with semimajor axes that are within 1 PSF length of each other in the outer part of the galaxy. These isophotes should have near identical fits, but noise in the data and non-axisymmetric features can cause deviations. It is those deviations that contribute to the uncertainty in PA and ellipticity as reported for the global fit.

2.5 Isophotal fitting

With background, PSF, centroid, and an ellipse (PA and ellipticity) initialization in place, AUTOPROF can fit elliptical isophotes to the galaxy image. For this isophotal fitting step, the default AUTOPROF function uses a method similar to J87 except with a modification taken from the field of machine learning. The latter improves upon speed and accuracy of the fitted results (see below). Machine learning is also used in other galaxy image analysis software, such as DEEPLEGATO (Tuccillo et al. 2018) and PIX2PROF (Smith et al. 2021). These methods incorporate more comprehensive machine learning-based pipelines, making them fast and accurate within their trained domain. AUTOPROF, on the other hand, provides a rich toolkit with additional user customizability and alternative output products such as those presented in Section 3. Thus AUTOPROF is ideally suited for a broad range of galaxy photometry tasks.

A series of elliptical isophotes with the global PA and ellipticity determined in Section 2.4 are constructed by growing geometrically in semimajor axis length from the centre (calculated in Section 2.3) until they approach the background level. The algorithm iteratively updates the PA and ellipticity of each isophote individually (in a random order) for many rounds. Each round cycles between three options: optimizing PA, ellipticity, and PA/ellipticity simultaneously. To optimize the parameters, a Monte Carlo method is used. New values for the current parameter (PA, ellipticity, or both) are randomly sampled with a small scatter around their current value. The 'loss' is now computed for the new parameters (PA, ellipticity, or both) and compared to the loss before scattering. The loss is a combination of the relative amplitude of $\mathcal{F}_2$[3] and a regularization term. The regularization term is borrowed from machine learning and penalizes adjacent isophotes for having a significantly different PA or ellipticity (using the l_1 norm). For the i^{th} isophote the loss is:

$$l = \frac{|\mathcal{F}_2|}{\tilde{\mu}+\sigma_b}\left(1+\frac{|e_i-e_{i-1}|}{1-e_{i-1}}+\frac{|e_i-e_{i+1}|}{1-e_{i+1}} + \frac{|p_i-p_{i-1}|}{0.2}+\frac{|p_i-p_{i+1}|}{0.2}\right) \quad (3)$$

where l is the loss to be minimized, N is the number of flux values sampled along the isophote, e_i and p_i are the ellipticity and PA of the ith isophote, respectively. The first factor in the loss function $\left(\frac{|\mathcal{F}_2|}{\tilde{\mu}+\sigma_b}\right)$ is nearly equivalent to the J87 optimization value, except that the denominator is adapted for robustness of the fit. The coupling between isophotes in the second factor takes the form of the l_1 norm (Shai Shalev-Shwartz 2014); the denominators $(1-e_{i\pm1}$ for e_i and 0.2 for p_i) are chosen to normalize the scale for the impact of parameter deviations. Thus, all the isophotes are coupled and tend to fit smoothly varying profiles.

For an intuitive understanding of the regularization term, consider an example where all the isophotes have been initialized to the same PA and ellipticity. If the ith isophote was to change PA by 0.2 radians (11.5°), then the regularization term would equal 3; meaning that the $\frac{|\mathcal{F}_2|}{\tilde{\mu}+\sigma_b}$ term would have to drop by more than a factor of 3 for the update to be accepted. While it is rare for two adjacent isophotes to differ by so much, this example demonstrates how the regularization term prevents the optimization routine from making extreme updates for minimal improvements in the fit. The exact choice of 0.2 as the regularization scale for PAs is not critical and near identical solutions will result from different choices of that scale. The user can also adjust the impact of the regularization term with a simple scale parameter; increasing the parameter for smoother fits, and decreasing it to allow for wider variability.

If the optimization completes three rounds without any isophotes updating, the profile is assumed to have converged. Fig. 5 shows an example isophotal solution (red solid lines) on a complex galaxy

[3]For comparison with the J87 method discussed in Section 4.1, we note that $\text{Im}(\mathcal{F}_2)=A_2$ and $\text{Re}(\mathcal{F}_2)=B_2$.

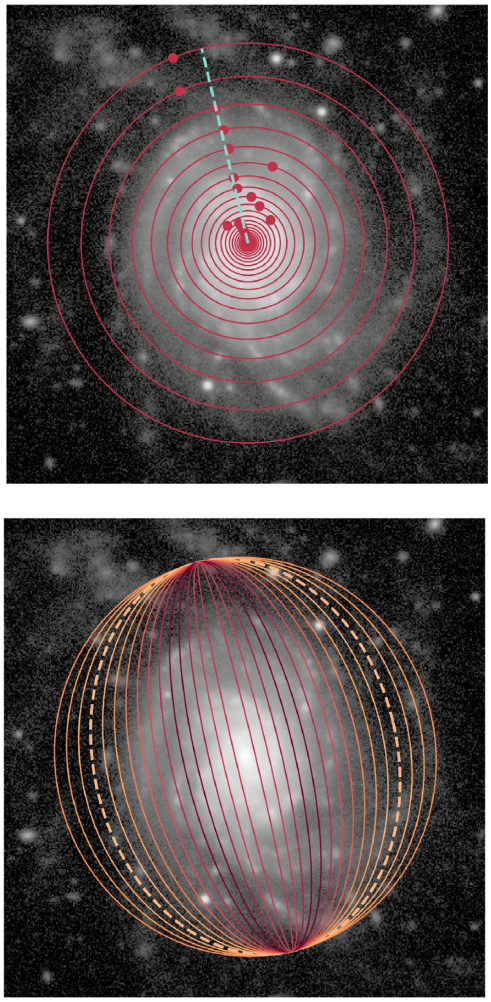

Figure 4. Isophote initialization procedure from the default AUTOPROF pipeline for *ESO479-G1*. Top: a global PA is determined by taking rings of flux (shown as red rings) and computing the phase of the $\mathcal{F}_1$ coefficient (red dots on the rings). The global PA is determined as the average direction for the outer five rings. Bottom: the global ellipticity is determined by testing a range of ellipticity values and computing $|\mathcal{F}_2/\mathcal{F}_0|$, where brighter colours represent lower values. The best candidate ellipticity (shown as a dashed line) is then further optimized using a Nelder-Mead minimization routine on $|\mathcal{F}_2/\mathcal{F}_0|$.

image. An uncertainty for each PA and ellipticity is determined by re-fitting 10 more isophotes at ±5 per cent of the semimajor axis length and taking the scatter in the fitted values.

Some codes enable 'deformed' elliptical isophote fitting through higher order Fourier modes. This is especially useful for early-type galaxies, which display discy or boxy structures, though its implementation can be taxing in an automated context. AUTOPROF does not currently include this capability, though the power in Fourier modes around the elliptical isophotes can be computed to arbitrary order.

Overlapping galaxies (merging or projected) will break the assumptions in this fitting scheme and may cause undefined behaviour in the resulting outputs. As AUTOPROF is not designed for the treatment of overlapping systems, such configurations are better suited for other methods (e.g. Section 4.3). AUTOPROF includes diagnostic checks (see Section 2.7) that aim at detecting such systems.

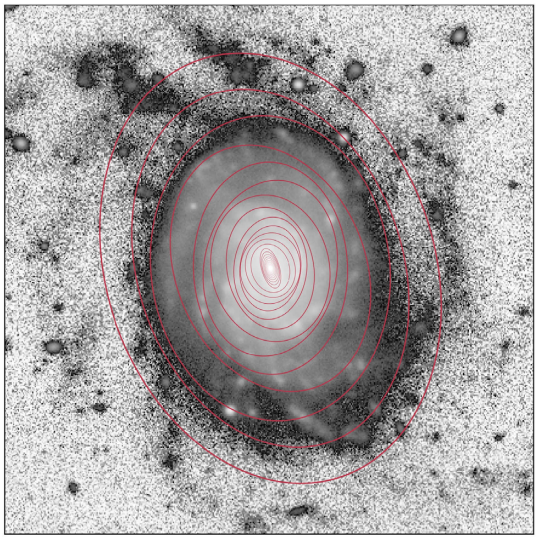

Figure 5. Example isophotal fitting solution for *ESO479-G1*. AUTOPROF tracks complex axisymmetric features even in the presence of many non-axisymmetric components such as spiral arms, H II clouds, and foreground stars.

2.6 SB profile extraction

Extracting reliable flux measurements from an image and maximizing S/N can be a challenging process. AUTOPROF approaches these goals in three steps. For galactocentric radii less than five times the PSF, the flux values change rapidly from pixel to pixel as central regions of galaxies are bright and centrally peaked. For this reason, AUTOPROF uses a Lanczos interpolation (default Lanczos-5 but this is user adjustable) between pixels to sample flux values exactly along each specified elliptical isophote (Shannon 1949; Burger & Burge 2010). This method samples pixel fluxes accurately, albeit slowly, along an isophote. For intermediate radii, where pixels have S/N > 2, the flux values are not assumed to change rapidly and a half pixel offset should not significantly affect the SB measurement. In this regime, fluxes are sampled from the nearest neighbouring pixel at regular angular separations (eccentric anomaly). For larger radii, where the S/N drops considerably, AUTOPROF samples a band of pixels around an isophote whose width is by default 5 per cent of the isophote radius. This method enables AUTOPROF to maximize S/N and reach low surface brightness (LSB) regimes. In the default configuration, isophote semimajor radii grow by 10 per cent so it is guaranteed that no pixel is counted twice (which would thwart the rigorous statistical interpretation of flux measurements and their uncertainty). The user may adjust the band width and radii growth scales arbitrarily and allow for overlapping isophotes; this produces artificially smoother profiles as the flux measurements will be correlated. This may or may not be an issue depending on the application. Also of note, because brightness profiles typically follow power-laws with semimajor axis, a large band relative to the power-law scale can bias flux measurements due to the inclusion of pixels which are not precisely at the desired radius. Here is another reason why band averaging is only used in the outskirts by default. Modelling the local power-law in brightness can allow users to mitigate the band averaging bias (Lauer 1986), though this feature is not included in AUTOPROF.

Once a band of pixels is selected, AUTOPROF computes the average flux using the median by default (though mean and mode are available). Additionally, AUTOPROF can perform sigma-clipping to

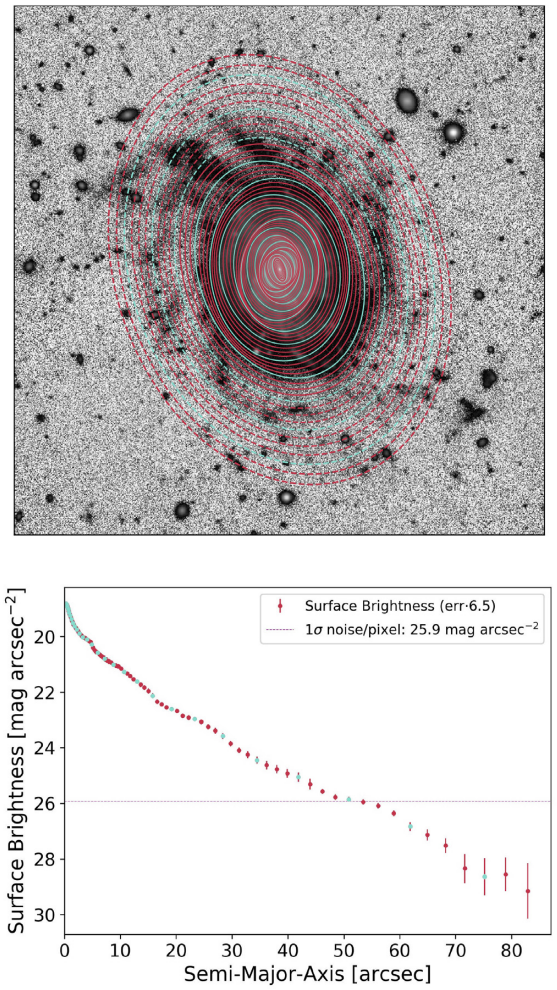

Figure 6. Diagnostic plots for the final SB profile of *ESO479-G1*. Top: sampling ellipses used for extraction of isophotal flux values. The dashed ellipses indicate extrapolation of the ellipticity and PA profile from the fitted values (extrapolated values are kept constant). Bottom: extracted median SB profile; cyan points (every fourth isophote) correspond to the cyan ellipses in the top figure facilitating visual comparison. The error bars have been scaled up to make them more visible; the scale factor is shown in the figure legend. The purple horizontal dotted line shows the estimated 1σ noise per pixel from Section 2.1.

remove bright sources along an isophote; users may take advantage of this feature in especially crowded fields (foreground stars, cluster environments, background galaxies on deep images, etc.). A segmentation map such as from SEXTRACTOR (Bertin & Arnouts 1996) or other masks can also be provided to remove unwanted sources from the flux extraction procedure. A carefully masked image should yield more reliable galaxy flux estimates (see Section 3.1), though sigma-clipping may produce comparable results.

Tests of forced photometry on generic regions of sky data (including cirri, stars, background galaxies, etc.) show that AUTOPROF can regularly achieve robust SB levels of $\sim$28 magarcsec^{-2} in the DESI *g*- and *r*-bands, and can often go even deeper in a clean environment (no large neighbour, no large contaminant such as a bright star). To achieve this level requires the sigma clipping feature; masks are also more effective. The limiting brightness is certainly a function of the sky environment and care must be taken when interpreting the results.

In order to track the total light within an isophote, AUTOPROF automatically includes two estimates of the total light; (i) an integral of the SB profile and (ii) a direct pixel summation. The direct pixel summation includes all non-masked pixels (masked pixels are flagged and never replaced by a numerical value). The SB profile integration is performed as:

$$f = 2\pi \int_0^R r I(r) q(r) \mathrm{d}r \tag{4}$$

where f is the total flux, R is the final semimajor axis of the integral, r is the semimajor axis over which the integral is performed, $I(r)$ is the flux as a function of semimajor axis, and $q(r)$ is the axial ratio as a function of semimajor axis. The integral is performed with the trapezoid method and has no treatment for overlapping isophotes. In principle, direct pixel summation should produce the most accurate total flux measurements. However, in practice, foreground objects and overlapping galaxies may alter this outcome. If these external sources are not carefully masked, the SB integral method is favoured for more reliable total flux measurements.

With the final isophotal solution in place, AUTOPROF in its default configuration generates a number of output products. The primary product, an SB profile, is a text file with a .prof extension. Such an SB profile can also be represented graphically, as shown in Fig.6. Table 1 gives a full description of the columns in the.prof output file; this information is also found in the GITHUB code repository. In addition to the SB profile, AUTOPROF generates a number of useful parameters for data quality checks and specific use cases. These extra checks and global image parameters are written to an auxiliary .aux file of the same name as the profile.

AUTOPROF can output a number of diagnostic plots for each operation. These plots allow the user to identify pathological cases that may disrupt isophotal fitting. Many of the figures in this paper are indeed examples of such diagnostic plots. A detailed description of all diagnostic plots can be found in the GITHUB code repository. In general, the plots favour diagnostic purposes over aesthetics and may magnify spurious features of the data.

2.7 Checking the fit

Various checks are applied to ensure that the isophotal fit has reached an acceptable solution. This is necessary in an automated analysis domain as large samples cannot be examined individually by a human, yet challenging or pathological cases may require extra attention. The latter may take multiple forms. For small- to mid-sized samples, a human operator may triage the identified problematic cases. For larger samples, one can take advantage of AUTOPROF's decision tree pipeline construction to modify settings and iterate until a suitable fit is achieved or it becomes clear that no reliable fit is possible. The checks described here are designed to flag cases in which the final fitted isophotes are not well described by a constant SB plus noise. This can happen for a variety of reasons including a fit which failed to converge, a misaligned centre, a bright foreground object, or a galaxy whose light distribution is poorly modelled by elliptical isophotes (Ciambur 2015). Here, we describe checks which AUTOPROF performs in its default configuration. Users may also implement their own checks for a particular application.

First, AUTOPROF compares the interquartile range of flux values along an isophote versus the median flux value. If over 20 per cent of the isophote have such variability, then the fit is flagged as having possibly failed. Secondly, AUTOPROF computes an FFT along the isophote and examines the power in the first-order mode. If 80 per cent of the isophotes have $|\mathcal{F}_1/(\tilde{\mu} + \sigma_b)| > 0.05$ or if

Table 1. Surface brightness profile output columns (.prof file).

Column (1)	Units (2)	Description (3)
R	arcsec	Isophote semimajor axis length
SB	mag arcsec^{-2}	Median SB along isophote
SB_e	mag arcsec^{-2}	Uncertainty on SB estimate
totmag	mag	Total magnitude enclosed in isophote, computed by integrating SB profile
totmag_e	mag	Uncertainty in totmag estimate propagated through integral
ellip	...	Ellipticity of isophote ($1 - b/a$)
ellip_e	...	Uncertainty in ellipticity estimate determined by local variability
pa	deg	PA of isophote relative to positive y-axis (increasing counter-clockwise) on the image
pa_e	deg	Uncertainty in PA estimate determined by local variability
pixels	count	Number of unmasked pixels sampled along isophote or within band
maskedpixels	count	Number of masked pixels rejected along isophote or within band
totmag_direct	mag	Total magnitude enclosed in current isophote by direct pixel flux summation

30 per cent have $|\mathcal{F}_1/(\tilde{\mu} + \sigma_b)| > 0.1$, then the fit is flagged. Thirdly, the same checks are performed except with the second Fourier coefficient ($\mathcal{F}_2$). The percentages and thresholds above were chosen by expert assessment with the goal of successfully capturing all cases that would be visually flagged for re-fitting. The flags may also capture a number of acceptable fits and may thus not be suitable for all situations/surveys. These checks are included to assist the user, however it may be necessary to create custom checks for a given application. These checks can serve as a starting point for more specialized versions.

2.8 Forced photometry

Forced photometry is the process of taking the isophotal solution (a profile of ellipticity and PA as a function of galactocentric radius) from one image and applying it to another image (generally taken at a different photometric bandpass). Forced photometry is critical for properly comparing colour measurements, since it forces consistent measurements at each pixel. It can also save on computation time as a galaxy should have a similar structure in other bands, ignoring the effects of dust, stellar populations, PSF, and sensitivity. Forced photometry can be used in cases where low S/N precludes the possibility of finding a robust fit, but where one expects a measurable signal.

In order to apply forced photometry, the user must provide a configuration file with the image file to process and a previously fit AUTOPROF profile. The default forced photometry pipeline is a modification of the default pipeline described above. The background level and PSF are re-calculated for each new image as in Sections 2.1 and 2.2, as these typically change from image to image. For centre finding, AUTOPROF uses the centre from the forcing profile, though a new centre can be fitted if needed. The global isophotal fitting in Section 2.4 is skipped and the forcing profile values are used instead. The isophote fitting step is no longer needed and skipped as well. The isophote extraction step proceeds as in Section 2.6 except that it now reads the PA and ellipticity values from the forcing profile and uses those as the set of isophotes to extract. The fitting checks in Section 2.7 are not run as no fitting is performed. The default forced photometry pipeline can, of course, be adapted and extended just as the regular photometry pipeline.

3 ADVANCED PIPELINE TOOLS

We now describe several analysis tools that complement the default AUTOPROF toolkit. These optional pipeline steps can be included in the configuration file. Users may also design their own pipeline by adding, removing, or reordering the steps in the default AUTOPROF pipeline. This may benefit special cases, fine tuning the analysis or adapting to the type of galaxy being analysed. The default functions, coupled with a flexible pipeline, make AUTOPROF well suited for a wide range of small and large scale galaxy photometry applications.

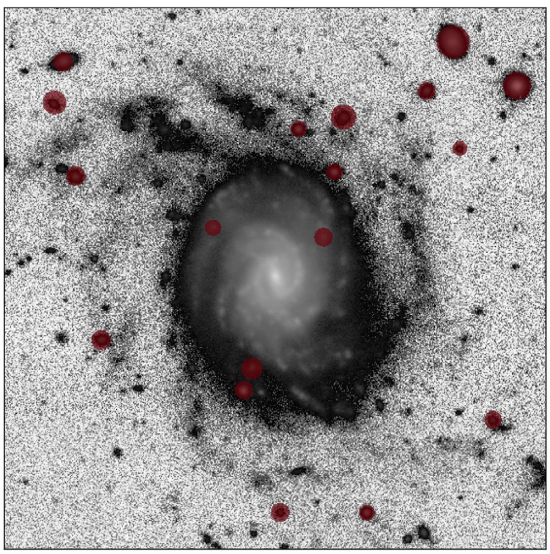

Figure 7. Example star mask method applied to *ESO479-G1*. The circular masks are adjusted in size based on the fitted FWHM for each star candidate. Typically two FWHM will be masked, though for bright objects this aperture increases logarithmicaly with the peak flux.

3.1 Star masking

In general, AUTOPROF can operate effectively without a mask as all procedures rely on robust mode, median, and percentile estimates of flux. However, the total luminosity, as reflected in the parameter 'totmag_direct' in Table 1, is directly affected by a lack of masking. Densely populated fields likely require that the galaxy image be masked appropriately before AUTOPROF processing to achieve reliable flux estimates. Built into AUTOPROF is a star finding algorithm (also used in Section 2.2), which identifies peaks using an edge detecting convolutional filter. AUTOPROF can automatically mask any identified star using the star finder (called 'starmask'). An example of such a mask is given in Fig. 7, here all identified star candidates are

masked regardless of deformity score (see Section 2.2) and the size of the mask is adjusted according to the individually fit FWHM. Note that the AUTOPROF star mask focuses on objects brighter than 10 times the noise of the background level. For more detailed masks on very faint stellar or extragalactic sources, which dominate the background in modern imaging surveys, the user may take advantage of more specialized masking tools (e.g. Bertin & Arnouts 1996; Akhlaghi 2019).

A mask can be provided by specifying the path to a fits file containing an image with the same dimensions as the galaxy image being studied. Any non-zero value in the provided file is considered a masked pixel. In the event that the user provides a segmentation map, such as the output from SEXTRACTOR (Bertin & Arnouts 1996), AUTOPROF will first identify the segmentation ID of the main galaxy using the centre from Section 2.3 and ensure that this ID is set to zero (i.e. not masked). The various mask options can be added sequentially via a logical-or operation.

3.2 Radial profiles

This complimentary tool in AUTOPROF (called 'radialprofiles') involves the extraction of light profiles along any axes PAs radiating from the galaxy centre (Courteau et al. 2011). Radial profiles (or wedges) typically trace the major or minor-axis of the galaxy (e.g. Fig. 8), though any orientation is possible. These radial profiles can be used to resolve axisymmetries that would otherwise be lost in azimuthal averaging,[4] examine dust distributions, disentangle thin and thick discs, and so on (e.g. Comerón, Salo & Knapen 2018). The computation of wedge profiles proceeds similarly to profile extraction in Section 2.6 except that flux measurements are a function of radius and angle instead of radius alone. By default, the radial wedges are sampled in four directions relative to the global PA of the galaxy, where each wedge is 15 deg wide as shown in Fig. 8. The number of wedges, orientation, and the width of the wedges can be defined by the user. Each profile will be sampled at the same radii as the semimajor axis values in the primary SB profile. Wedges with exponentially growing widths (Courteau et al. 2011) that maintain constant S/N ratios are also available. Similarly, wedges with variable PAs that follow complex features near the centre (bar or spiral arms) can also be modelled. Radial wedges are provided as an advanced option and are not activated by default.

3.3 Axial profiles

Another tool provided by AUTOPROF, called 'axialprofiles', is the extraction of axial SB profiles (Comerón et al. 2018) along lines parallel to a chosen axis (typically the major or minor-axes). These slices can be used to study the same features as radial wedges but keeping their widths constant and allowing offsets from the galaxy centre.

Fig. 9 displays every fifth sampling line and resulting profiles for one quadrant on *ESO479-G1*. The spacing between axial profiles (and their width) grows geometrically by default, allowing AUTOPROF to collect more signal in fainter regions of the galaxy. Along each axial profile, the bin sizes grow geometrically to increase S/N as the profile moves away from the primary axis (as can be seen by the spacing between points in Fig. 9).

[4]Standard isophotal analysis, or surface photometry, is not valid for edge-on galaxies as the entire disc is projected along the line of sight.

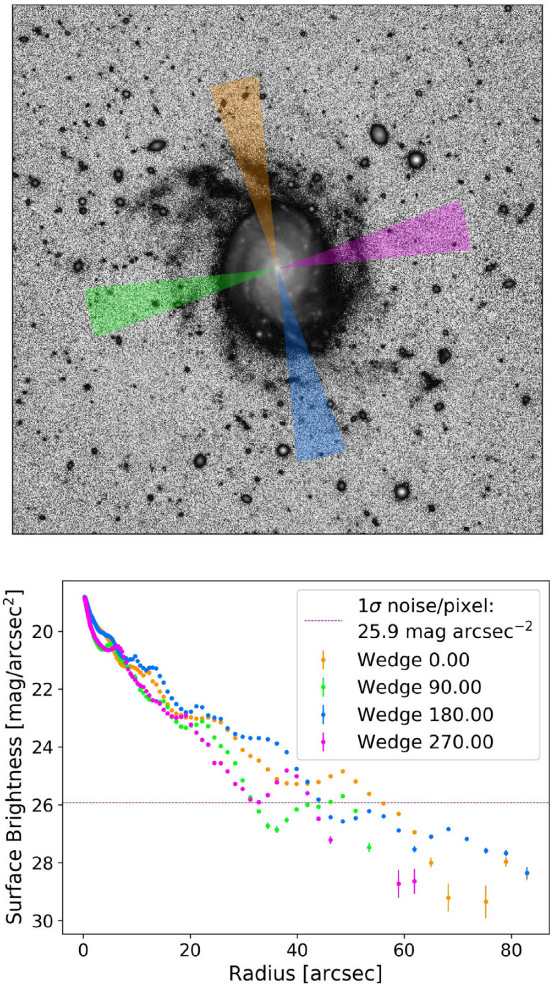

Figure 8. Example: radial profile wedges for *ESO479-G1* demonstrating which parts of the image are sampled for each wedge. Top: visualization of sample extraction; the blue/orange wedges trace the semimajor axis, while the pink/green wedges trace the semiminor axis. Bottom: resulting radial SB profiles showing features along each wedge.

3.4 Ellipse model

Another AUTOPROF tool (called 'ellipsemodel') generates smooth 2D models of galaxies based on AUTOPROF's 1D SB profile; this is saved to a FITS file with the same dimensions as the original image. There are two possible ellipse model modes. In the simplest mode, the image is stretched along the minor-axis until the global ellipse fit (Section 2.4) is circular in the transformed space. The 'SB_fix' column of the SB profile is interpolated at the radial location of each pixel and assigned the corresponding interpolated flux value. The more general ellipse model shown in Fig. 10 is constructed like the fixed ellipse model. The latter is repeated for each isophote in the SB profile using its individual PA and ellipticity values. Each pixel uses the corresponding values from the closest ellipse once all iterations have been completed.

For both the fixed and the general ellipse models, no extrapolation of the SB profile is performed. Instead all flux values beyond the outer isophote are set to zero. This can be seen in the middle image of Fig. 10 in the sharp transition to the black background.

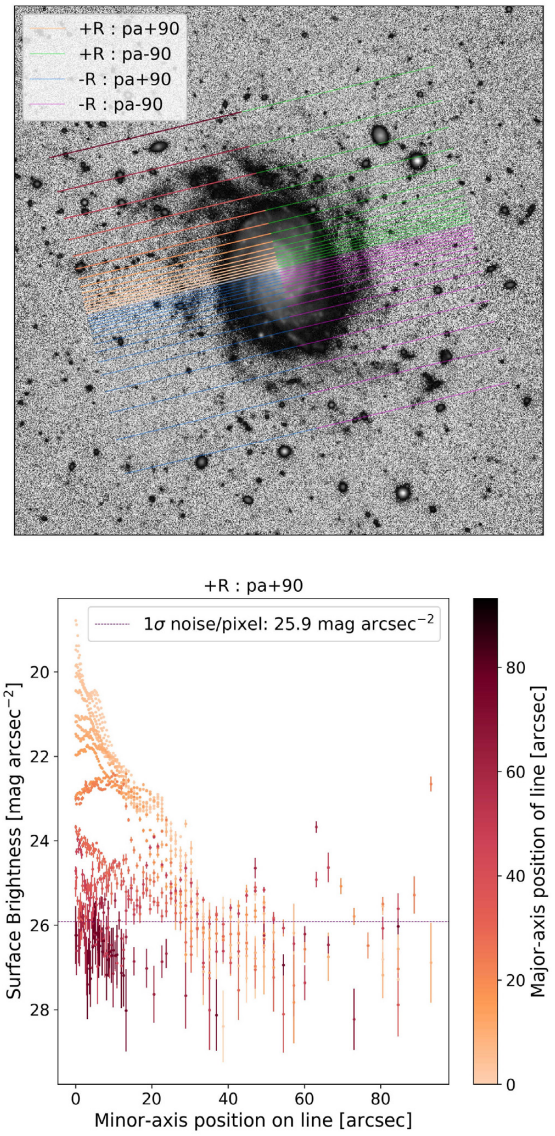

Figure 9. Example of AUTOPROF axial profiles on *ESO479-G1*. Top: projection of axial profile lines parallel to the minor-axis on the galaxy image. Colours indicate what quadrant of the galaxy is being sampled. Bottom: Resulting set of axial profiles for one quadrant (orange lines of top panel) of the top figure. The x-axis is the distance from (in this case) the major-axis of the galaxy, and the colour scale now indicates the starting point for each sampling line from the galaxy centre along the major-axis.

3.5 Fourier mode analysis

AUTOPROF includes two tools for examining higher order information on fitted isophotes. The first and simplest available method measures the Fourier mode power spectrum along an ellipse. During the isophote brightness extraction step (see Section 2.6), AUTOPROF can perform an FFT decomposition along each ellipse and measure the power in each mode. These are reported relative to the zeroth coefficient, which roughly corresponds to the mean flux along an isophote; the real and imaginary parts of the coefficient are given as $\frac{B_n}{F_0}$ and $\frac{A_n}{F_0}$, respectively. The fourth mode, F_4, is commonly used to measure the boxyness/disciness of an isophote, whilst the low odd modes, F_1 and F_3, are commonly used to measure asymmetry in a galaxy (Peng et al. 2010).

In some cases, it is not sufficient to measure the Fourier modes along elliptical isophotes; instead a fit is needed to include these perturbations in the isophote. This can occur for boxy/discy galaxies, or very lopsided galaxies where the contours of constant SB depart from an elliptical shape. AUTOPROF provides built in functionality to fit isophotes as ellipses with user selected cosine perturbations. The perturbation for each mode is described by two parameters, A_m and ϕ_m, which control the amplitude and phase respectively for each mode m. The exact form of these perturbations is given in equation (5).

$$R(\theta) = R_0(\theta) e^{\sum_m A_m \cos(m(\theta+\phi_m))}, \tag{5}$$

where R_0 is the radius for a traditional ellipse and R is the radius of the perturbed isophote. Note that the sum is only performed over user selected modes, thus it is possible to construct an isophote using only e.g. fourth-order perturbations. In other implementations, the form of the perturbation in equation (5) would be $R_0(\theta)(1 + \sum_m A_m \cos(m(\theta + \phi_m)))$ assuming A_m is small (e.g. Peng et al. 2010). However, this has the undesirable feature of becoming negative if an A_m, or some combination of them, is greater than 1. Whilst this is unlikely to occur in real cases, an optimization algorithm may fail if part of the parameter space is invalid. Thus, we use $e^{\sum_m A_m \cos(m(\theta_m+\phi_m))}$, which is always positive and for small amplitudes, it is equivalent to other implementations ($e^x = 1 + x + \mathcal{O}(x^2)$).

As more parameters are added to the fitting procedure, AUTOPROF can model more complex systems. However the increased parameter space naturally also increases the likelihood of fitting spurious image features, causing worse performance overall. To combat this, we extend the loss function described in Section 2.5 to now include regularization terms for the cosine perturbations:

$$\begin{aligned} l = \frac{\sum_{2,m}[|\mathcal{F}_m|]}{\tilde{\mu} + \sigma_b} \Bigg(1 + \frac{|e_i - e_{i-1}|}{1 - e_{i-1}} + \frac{|e_i - e_{i+1}|}{1 - e_{i+1}} \\ + \frac{|p_i - p_{i-1}|}{0.2} + \frac{|p_i - p_{i+1}|}{0.2} + \sum_m \Bigg[\frac{|A_{m,i} - A_{m,i-1}|}{0.2} \\ + \frac{|A_{m,i} - A_{m,i+1}|}{0.2} + \frac{|\phi_{m,i} - \phi_{m,i-1}|}{0.1m} + \frac{|\phi_{m,i} - \phi_{m,i+1}|}{0.1m} \Bigg] \Bigg) . \end{aligned} \tag{6}$$

Note that the first sum now includes the user selected modes, m, and the second Fourier mode; the sum in the regularization term only goes over the user selected modes. For the $\phi_{m,i}$ terms in the regularization scale, the factor m in the denominator reflects the reduced angular range of the higher mode perturbations (a full cycle completes every $\frac{2\pi}{m}$ radians). All other standard AUTOPROF methods will automatically adapt to the new higher order isophotes. The isophote flux sampling procedures described in Section 2.6 will now accept the more complex isophote shapes, which may result in better error performance as the brightness is more uniform along each isophote. However, the interpretation of the measurements (and even the semimajor axis) can be more challenging.

The resulting fitted isophotes are stable, even with high frequency modes. However, the runtime for fits with these perturbations is considerably longer, often taking twice as long to converge. The resulting isophotes follow contours of constant SB more closely than ellipses alone, as can be seen in Fig. 11 which was fitted using modes 1, 3, and 4. There is a clear lopsidedness to the galaxy at larger radii; at small radii, the perturbations allow AUTOPROF to follow the spiral arms contours. This added complexity may or may not provide added insight. In general, users should use the cosine mode fitting with intention, only fitting when a signal is expected. For example, with the fourth mode to early-type galaxies, or with the first and

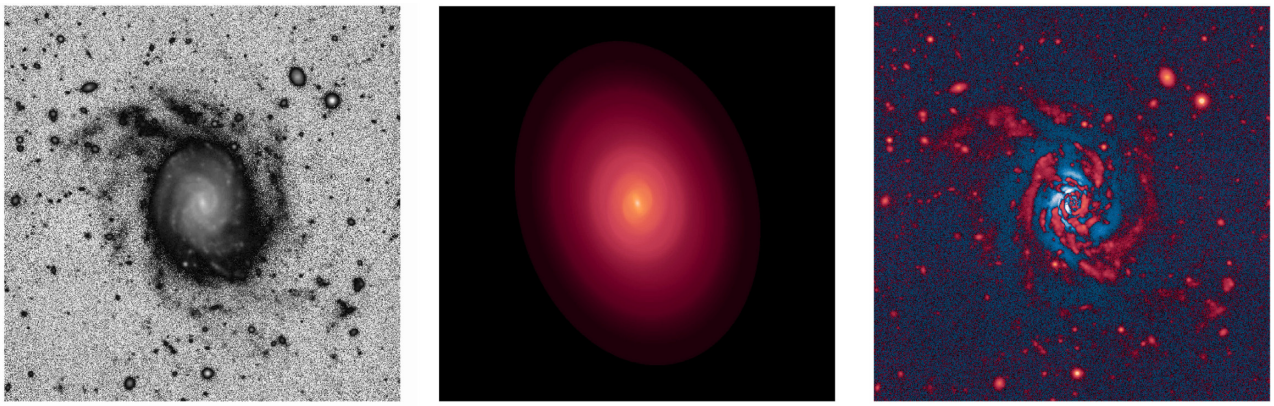

Figure 10. Left: image of *ESO479-G1*. Middle: example smooth ellipse model of flux values for *ESO479-G1* demonstrating the constructed model. Colours follow a log scale flux and show how the smoothed model handles variable PA and ellipticity values along the profile. Right: residual plot with ellipse model subtracted from original image. Blue colours indicate negative values and red colours indicate log-scale positive values.

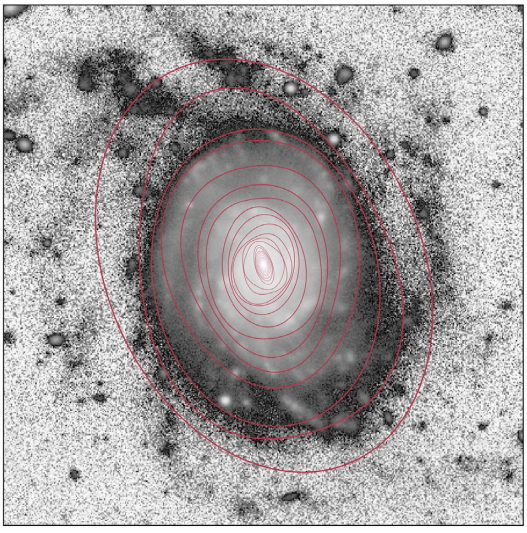

Figure 11. Example of fitted isophotes with higher mode perturbations, formatted as in Fig. 5. Isophotes follow contours of constant SB more closely, at the cost of increased complexity. Here, AUTOPROF has fitted first-, third-, and fourth-order perturbations to a standard ellipse, with the outer isophotes primarily using the first and third modes to model the galaxy asymmetry, while the inner isophotes primarily use the fourth mode to track spiral features.

third modes for searches of lopsided features (i.e. tidal streams). The second mode is also partly degenerate with the ellipticity and should thus be avoided in typical scenarios.

The two methods available in AUTOPROF for evaluating higher order information should, in principle, yield identical results; in practice, this is not the case. The fitted perturbations sample new parts of an image compared to simply measuring the Fourier amplitudes along an ellipse, thus the two techniques are evaluated on different information. Further, the fitted perturbations only model the selected modes, and thus they may 'wash out' some information which could be expressed in other modes. Each method will also be impacted by noise and foreground objects differently. Finally, attempting to use both methods simultaneously will invalidate the Fourier amplitude measurement method as it will no longer apply to an ellipse, but rather to a more complex isophote. Thus, it is best to select the method which best suits a given application and solely apply it to the images.

3.6 Decision tree pipelines

In addition to AUTOPROF's toolkit, users can implement decision trees in order to run specific applications on separate galaxy images. For instance, one may wish to extract different data from edge-on versus face-on galaxies, early- versus late-type galaxies, crowded fields versus isolated galaxies, large versus small extent on the sky, and so on. Another application is to re-analyse a galaxy which fails the fit checks (Section 2.7) using alternate settings in an attempt to recover an accurate ellipse model. An example flow chart, shown in Fig. 12, demonstrates two types of decision tree choices. The decision tree is provided through the configuration file and an example is included with the code to support initial development. AUTOPROF decision trees can be arbitrarily complex and integrate user-defined functions.

4 COMPARISONS WITH OTHER METHODS

To demonstrate the accuracy of AUTOPROF data products, we compare our results to similar surface photometry image analysis software. For these comparisons, we compare with the non-parametric packages PHOTUTILS (Bradley et al. 2020) and XVISTA (Lauer 1985), as well as the parametric decomposition software GALFIT (Peng et al. 2010). This is not an exhaustive comparison of isophotal fitting codes, others include ELLIPSE (Tody 1986), GIM2D (Simard et al. 2002), PYMORPH (Vikram et al. 2010), GALAPAGOS (Barden et al. 2012), IMFIT (Erwin 2015), and ISOFIT (Ciambur 2015) to name a few. Clearly, modelling galaxy light profiles is an active field in extra-galactic astronomy.

To establish the relative performance of AUTOPROF and other methods, we take advantage of 1387 late-type galaxies from the 'Photometry and Rotation Curve Observations from Extragalactic Surveys' (PROBES) catalogue (Stone & Courteau 2019; Stone, Courteau & Arora 2021). The PROBES galaxy images were extracted from the DESI-LIS Data Release 9 (Dey et al. 2019), which provided deep photometry in g, r, and z photometric bands. All results are computed in the r-band unless otherwise indicated. The comparisons below should serve to adequately present AUTOPROF in the context of available codes.

Our comparisons have also included measures of the relative run times for each method. Their interpretation is however thwarted by operational considerations unique to each method (e.g. we initialize PHOTUTILS with AUTOPROF pipeline functions). The runtime also varied considerably with user tunable parameters and the conditions

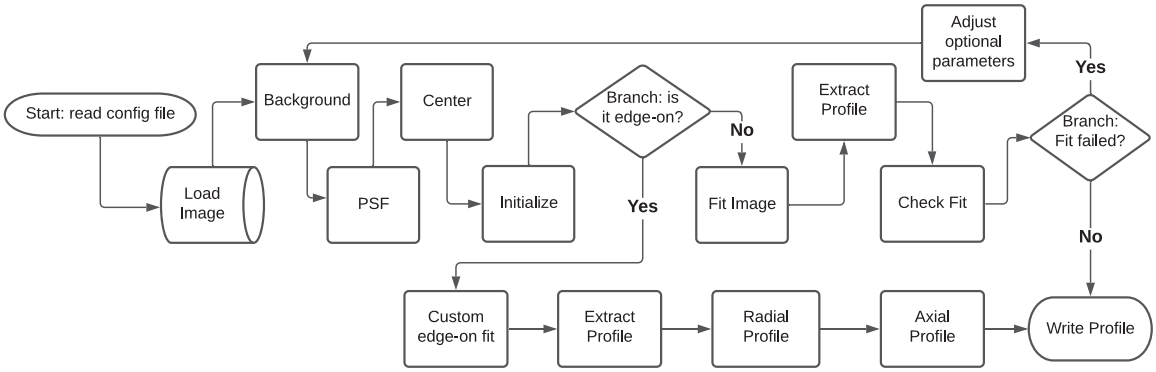

Figure 12. Example of an AUTOPROF decision tree flowchart. There are two instances where the 'branches' make a decision (indicated by rhombus blocks). If an edge-on galaxy is encountered, a specialized analysis pipeline can be applied. If the fitting procedure in the standard pipeline fails, the branch can update parameters and perform the fit again. The decision tree is fully adaptable and expandable.

of each image. Still, the general trend shows that the automated approaches (PHOTUTILS, AUTOPROF, and GALFIT) have comparable runtimes, while interactive methods (XVISTA) are slower by orders of magnitude (Smith et al. 2021)

4.1 PHOTUTILS

The PHOTUTILS package includes a variety of methods for analysis of astronomical images (Bradley et al. 2020). Included in the package is an implementation of the iterative isophotal fitting method by J87, which performs a weighted least squares fit of the intensities along an isophote according to:

$$I(\phi) = I_0 + A_1 \sin(\phi) + B_1 \cos(\phi) + A_2 \sin(2\phi) + B_2 \cos(2\phi) \quad (7)$$

where $I(\phi)$ is the intensity at angle ϕ around the isophote, I_0 is the average intensity around the isophote, and the A_n, B_n are Fourier coefficients with n indicating the order of the coefficient. The properties of the isophote are iteratively updated until the Fourier coefficient amplitudes are below 4 per cent of the RMS scatter of the intensities (or the maximum number of iterations is reached).

This technique reliably produces isophotes for smooth systems (e.g. typical elliptical galaxies). However, the possible presence of strong non-axisymmetric features violates the method's assumptions and can produce chaotic isophotal solutions. Interactive corrections of such chaotic isophotal solutions are enabled in XVISTA, as discussed in Section 4.2.

For the PHOTUTILS implementation of the isophotal solving technique in J87, an initial ellipse with a reasonable first guess for the PA and ellipticity are required. To perform a robust comparison, we make use of the AUTOPROF pipeline, replacing the isophotal fitting scheme in Section 2.5 and the isophote extraction scheme in Section 2.6 with their PHOTUTILS counterparts. The flexibility of the AUTOPROF pipeline design allows us to easily interchange individual segments for the sake of comparisons. This makes for a clean comparison between the two methods as all pre-processing steps are identical.

Fig. 13 shows a comparison of the SB profiles from PHOTUTILS and AUTOPROF applied to all PROBES galaxies; including only cases where both methods successfully converged on a solution. The four difference panels show that the median fitted value for SB, PA, and axis ratios are nearly identical for AUTOPROF and PHOTUTILS out to $2R_{23.5}$. This is expected as both methods are based on the same J87 method. The curve of growth comparison shows PHOTUTILS as dimmer near the centre and systematically brighter past $\sim 1.5R_{23.5}$. The extra light is due to the PHOTUTILS curve of growth being

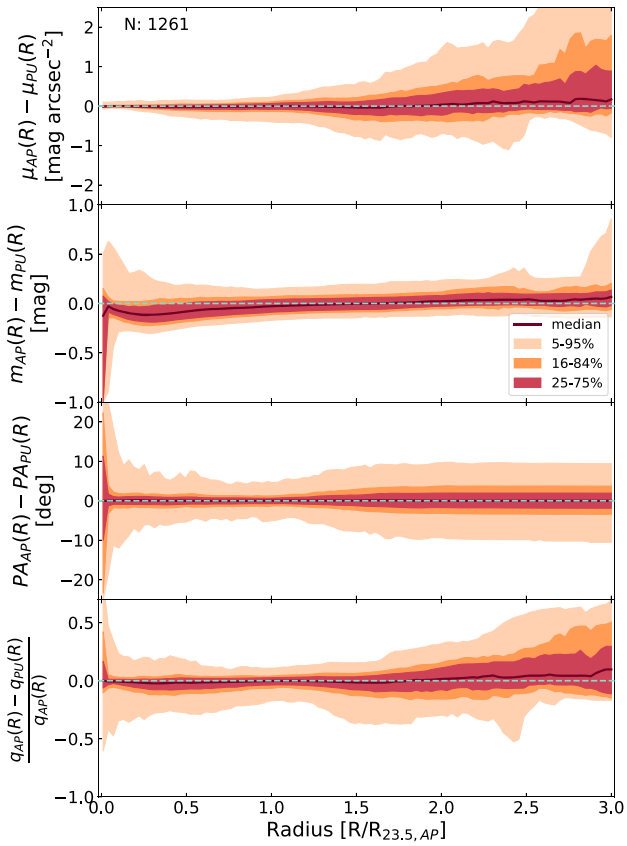

Figure 13. Comparison of photometric profiles from AUTOPROF and PHOTUTILS. Subplots show differences in the SB, curves of growth, PA, and axial ratio measurements, respectively. The solid dark line represents the median deviation as a function of radius, and the cyan dashed line gives zero as a reference point. The contours enclose 50, 68.3, and 90 per cent of the parameter comparisons at each radius, as indicated in the legend. The number of compared galaxies, N, is shown in the upper left corner of the upper panel.

based on pixel flux summation, which will be biased high from unmasked sources. Beyond $2R_{23.5}$, PHOTUTILS reports systematically narrower and brighter isophotes. Our AUTOPROF analysis included sigma-clipping of the SB measurements, removing most of the brightness bias due to foreground sources, yielding dimmer SB

measurements. Some deviations in the curve of growth and axial ratio also exist at very small radii. Indeed, the inner few isophotes can be significantly impacted by small pixel fluctuations causing swings in PA and ellipticity values. AUTOPROF combats these small radii effects by using its regularization scale and only fitting down to one PSF radius, however the issues occur for both AUTOPROF and PHOTUTILS fits. The choice of interpolation scheme also plays a role in profile differences for the central regions; AUTOPROF uses Lanczos interpolation while PHOTUTILS uses a less accurate Bilinear method. Comparison showed that the two methods can return differing flux estimates by over 5 per cent, although it varies considerably from case to case.

At large radii, beyond $R_{23.5}$, the scatter for the axial ratio and SB comparison increases markedly due largely to differences in low S/N behaviour. The J87 method can acquire deviations from non-axisymmetric features (e.g. unmasked stars may play a role at these low SB levels), whereas AUTOPROF is stabilized by the regularization term. Appendix B shows specific cases of disagreement between the methods.

AUTOPROF applies band averaging to determine the average flux for outer isophotes, the degree to which this technique improves the *S/N* is dependent on the size of the band and of the galaxy on the sky. The band averaging method can produce significant gains over direct sampling along an isophote. To quantify the improvement, we can compare the photometric depth achieved by AUTOPROF and PHOTUTILS. in Fig. 14, we show deepest SB levels for AUTOPROF and PHOTUTILS before reaching a nominal error limit of 0.2 magarcsec^{-2}. Thanks largely to the band averaging method, AUTOPROF can reliably achieve a 2 magarcsec^{-2} improvement over PHOTUTILS and in many cases reach even deeper. Factors other than the band averaging also contribute to achieving deep SB levels. AUTOPROF determines its errors with $\frac{\Delta_{16}^{84}}{2\sqrt{N}}$, whereas PHOTUTILS uses $\frac{\sigma}{\sqrt{N}}$. For Gaussian noise these measures are identical, however in the presence of outliers (foreground stars and background galaxies) the PHOTUTILS errors are biased high relative to AUTOPROF. Some of the more extreme SB differences (e.g. Δmag arcsec$^{-2} \approx 8$) stem from error-based stopping criteria in PHOTUTILS fits, which can terminate a profile in the central regions if a foreground star or an irregular galaxy feature (e.g. bright H II region, spiral arms, or dust lanes) is encountered.

4.2 XVISTA

The XVISTA photometry package[5] offers a wide range of image processing tools. We focus on the galaxy surface photometry analysis, which uses low-order Fourier coefficients (much like J87) to iteratively fit elliptical contours of constant SB (Lauer 1985; Courteau 1996; McDonald et al. 2011; Hall et al. 2012; Gilhuly & Courteau 2018). Included in XVISTA's surface photometry package are extra steps for manual adjustment of the isophotal solution after basic profile fitting. Here, the user examines the radial profiles of SB, PA, and ellipticity to identify problematic regions, and interpolates between robust regions to fill problematic areas. The resulting profiles represent the large-scale structure of the galaxy with high fidelity, without the influence from small non-axisymmetric features (and guards against the possibility of crossing isophotes). Provided close attention, XVISTA allows for an accurate non-parametric elliptical representation of the light distribution of a galaxy. Profile interpolations may also remove some fine structure in the fit, but the global light distribution is always preserved (Lauer et al. 2005). The primary drawback of this method is the lack of scalability if human intervention is involved.

[5] http://astronomy.nmsu.edu/holtz/xvista/index.html

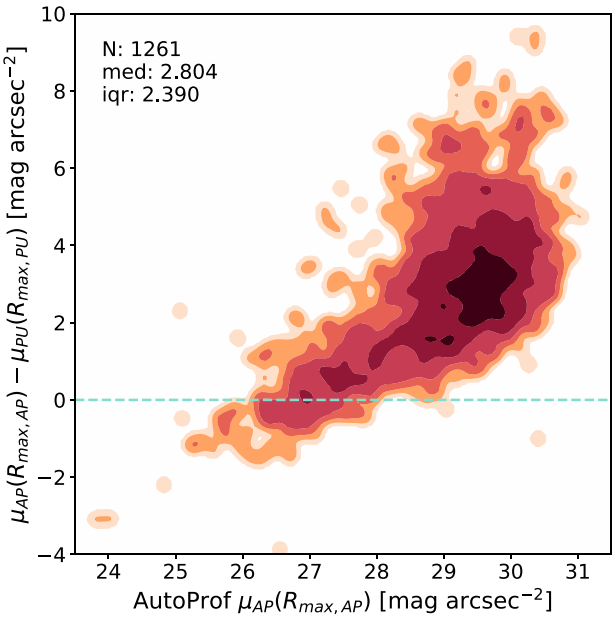

Figure 14. Comparison of photometric depth achieved by AUTOPROF and PHOTUTILS. The *x*-axis shows the deepest isophotes in the AUTOPROF photometry before reaching an error limit of 0.2 magarcsec^{-2}. The *y*-axis shows the SB difference between the AUTOPROF and PHOTUTILS deepest isophotes (before reaching an error of 0.2 magarcsec^{-2}). The contours represent the density (log scale) of galaxies. The cyan dashed line indicates zero difference in photometric depth.

We have applied the XVISTA surface photometry analysis to a sample of 722 PROBES galaxies for comparison with AUTOPROF profiles. These were all extracted uniformly by one of us (NA). The XVISTA surface photometry package includes its own methods for background subtraction, star masking (also done manually), SB extraction, etc (Courteau 1996). Thus our comparison with XVISTA will be influenced by differences in all of these steps, as well as the actual isophotal fitting routine. XVISTA and AUTOPROF are indeed fully independent of each other. Despite these caveats, Fig. 15 shows remarkable agreement between AUTOPROF and XVISTA. Our SB estimates are reliably equivalent to within less than 0.3 magarcsec^{-2} out to the outskirts ($\sim 3R_{23.5}$) of each galaxy. There is a slight bias beyond $R_{23.5}$ for AUTOPROF to have dimmer isophotes (by 0.03 magarcsec^{-2}) which may be explained by both AUTOPROF and XVISTA applying the technique of extrapolating the outer fitted isophote, each using a different point to select the last isophote. The slight brightness difference could also arise from a different masking procedures, where XVISTA uses manually created object masks and AUTOPROF uses sigma clipping. The curve of growth and PA profiles are remarkably tight over the entire range tested. Note that XVISTA nominally defines PAs relative to the positive *y*-axis and increasing clockwise; we inverted this for the sake of comparison. The axial ratio comparison shows a slight systematic shift beyond $R_{23.5}$ indicating that AUTOPROF finds rounder isophotes by approximately 2 per cent (median deviation past $R_{23.5}$).

A comparison of LSB features is also most instructive. Fig. 16 shows a comparison of photometric depths between XVISTA and AUTOPROF before encountering a SB error of 0.2 magarcsec^{-2} limit. For the same data, AUTOPROF's SB profiles reach deeper SB levels

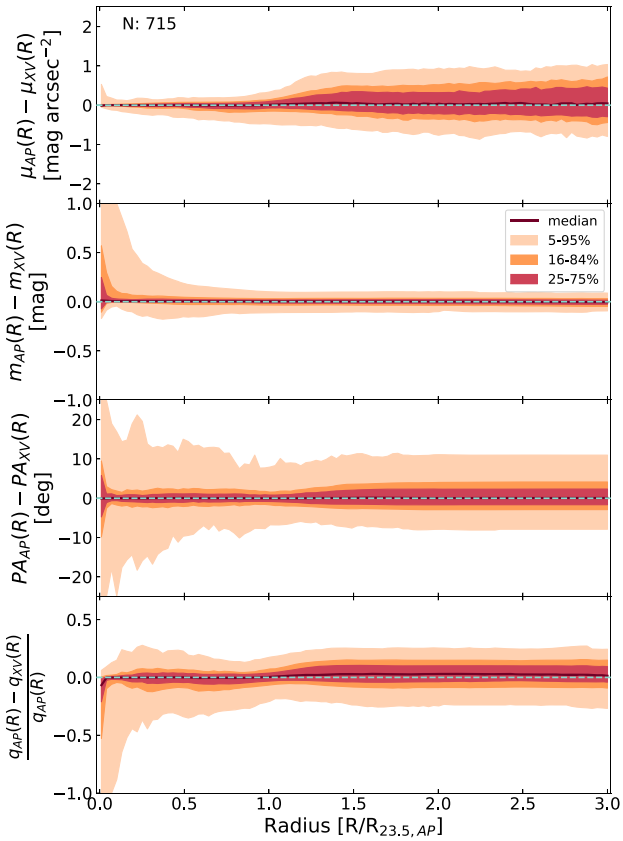

Figure 15. Same as Fig. 13 for comparing radial profiles from AUTOPROF and XVISTA.

since AUTOPROF uses band averaging in the outskirts (Section 2.6). AUTOPROF typically achieves deeper photometry by ~ 1 magarcsec^{-2} and can often reach deeper levels by more than 2 magarcsec^{-2}. Note that XVISTA computes errors similarly to PHOTUTILS using $\sigma/\sqrt{N}$ and is biased high by unmasked sources.

4.3 GALFIT

GALFIT performs structural decompositions of galaxy images with parametric 2D light distributions (Peng et al. 2010). Comparisons of structural parameters derived with AUTOPROF and GALFIT have already been performed in Arora et al. (2021) using PYMORPH, here we will compare profiles directly. GALFIT's parametric approach to modelling galaxy images is fundamentally different from AUTOPROF, PHOTUTILS, and XVISTA. Through least squares optimization, GALFIT can extract an arbitrary number of parametric models to fit a galaxy image. These models include the exponential disc (de Vaucouleurs 1958; Freeman 1970; Kormendy & Bruzual 1978; Kent, Dame & Fazio 1991; van der Kruit & Freeman 2011), Sérsic (Sérsic 1968), Moffat (Moffat 1969), Nuker (Lauer et al. 1995), and others. A PA and ellipticity are fit for each component globally. GALFIT models are typically azimuthally represented as an ellipse, though they can be transformed to fit boxy, pointed, twisted, and more shapes. GALFIT can also create especially detailed models,[6] more so than elliptical non-parametric fits. With manual fine-tuning and well chosen initial conditions, GALFIT models can describe a galaxy's

[6]see https://users.obs.carnegiescience.edu/peng/work/galfit/README.pdf

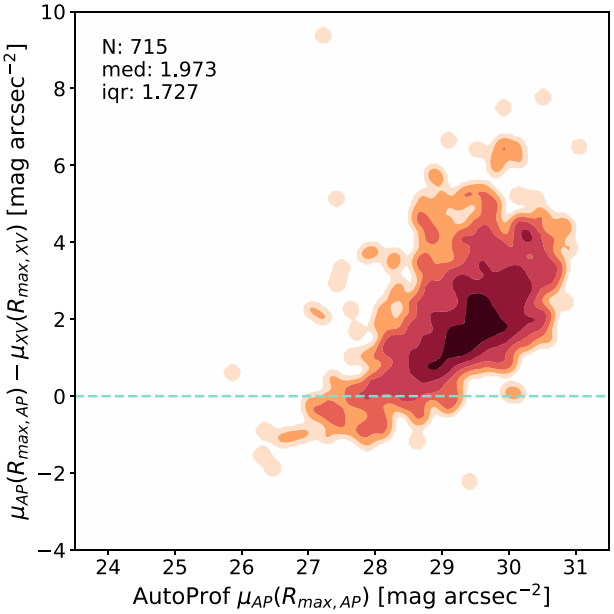

Figure 16. Comparison of photometric depths achieved by AUTOPROF and XVISTA; formatted as in Fig. 14.

light distribution with high fidelity, relative to the other methods considered here (AUTOPROF, PHOTUTILS, and XVISTA). The user can extract detailed information about individual features such a bulge, bar, spiral arm, etc, by first modelling the whole galaxy then either focusing on a single component or subtracting various components by choice. As such, one may investigate galaxy structure in a fundamentally different way than in elliptical non-parametric fits, making the methods highly complimentary. However, the process of constructing, such a detailed model is time consuming and its efficient and reliable implementation for large surveys can be challenging. For large surveys, GALFIT has been used in an automated fashion with one or two component models to fit galaxy images (e.g. Kelvin et al. 2010; Simard et al. 2011). Such models are well suited for low resolution images, and for overlapping systems where all sources in the image can be simultaneously modelled.

Since AUTOPROF is intended for scalability without user input on a per galaxy level, our comparison of the two methods uses simple two-component GALFIT models consisting of combinations of Sérsic and exponential disc profiles. We have applied those GALFIT parametric models to the our PROBES sample of galaxies. The GALFIT fitted models are sensitive to parameter initialization, owing partly to the overly simplistic choice of the two component models. To start the models with the closest approximation to their final values, we used the results from the AUTOPROF pipeline to construct GALFIT configuration files. The non-parametric AUTOPROF SB profiles were decomposed into Sérsic and exponential components using a least squares optimization to the 1D profiles. The resulting parameters were then given as initialization for GALFIT, along with the global PA and ellipticity fitted to the image. GALFIT is also sensitive to un-modelled image components. We therefore applied SEXTRACTOR (Bertin & Arnouts 1996) to build a segmentation map and mask all non-galaxy components of the image (mostly stars and background galaxies). The initialization for the component centres were taken from the AUTOPROF pipeline. We constructed a PSF for each image using a median of many flux-normalized stars (selected using the AUTOPROF star finder from Section 2.2). Each galaxy was

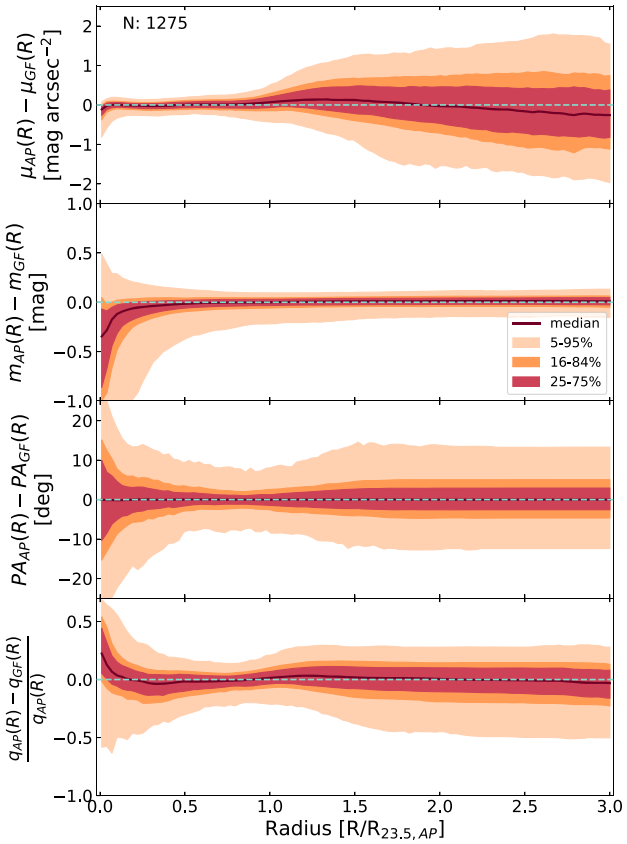

Figure 17. Same as Fig. 13 for the comparison of radial profiles from AUTOPROF and GALFIT.

modelled with (i) an exponential disc, (ii) a Sérsic function, (iii) an exponential disc and a Sérsic, and (iv) a doubleSérsic. The adopted model was the one with lowest χ^2/dof as reported by the GALFIT fitting routine (e.g. Simard et al. 2011; Gilhuly & Courteau 2018).

GALFIT models must be converted into SB profiles for proper comparison with AUTOPROF's output. This is accomplished by applying AUTOPROF to the final, idealized, GALFIT model. Fig. 17 shows a comparison of the resulting photometry profiles. Within $R_{23.5}$ the match between AUTOPROF and GALFIT is good. Larger systematic deviations are seen beyond $R_{23.5}$. At most radii, the scatter around the zero line is larger than in the comparisons with PHOTUTILS and XVISTA; this is to be expected given our choice of a two component model. Simple models fail to capture the full complexity of the late-type galaxy population in PROBES; a multicomponent model could yield better results at the expense of scalability. While the curve of growth comparison is poor in the centre, it converges quickly and remains good out to $3R_{23.5}$. A mismatch at the centre is expected and occurs on the PSF scale (roughly $0.2R_{23.5}$ on average) where isophotes are rounded. PA comparisons show no systematic differences throughout the profiles, however the random scatter is considerably larger than with PHOTUTILS and XVISTA (see Sections 4.1 and 4.2). The PA scatter is most pronounced near the centre where non-axisymmetric structures, such as bars can have PAs offset from the global PA; GALFIT could only recover the global PA using simple two component models. The axial ratio profiles show AUTOPROF finding systematically rounder values near the centre as expected due to the PSF scale ($\sim 0.2R_{23.5}$) which affects AUTOPROF results, but not GALFIT since it models the PSF. At large radii where axis ratios are more stable, AUTOPROF and GALFIT agree with no bias, albeit with a larger scatter than PHOTUTILS and XVISTA. Overall, both methods adequately match the global light distribution of each galaxy. However, GALFIT is restricted to two 'rigid' model components and thus cannot account for variations in PA and ellipticity. Being unable to account for those, GALFIT must 'split the difference' which ultimately leads to a larger scatter in all profile parameters. More detailed multicomponent GALFIT models can match galaxy images with greater fidelity and likely better agreement with AUTOPROF radial profiles of SB, PA, and ellipticity. An advantage of the non-parametric ellipse fitting approach in AUTOPROF (and similar codes) is that it is nearly equivalent to fitting many parametric models simultaneously allowing for more complete representation of the light distribution.

5 CONCLUSION

We have presented the robust automated isophotal solving pipeline, AUTOPROF for the extraction of valuable structural information from galaxy images. The pipeline is easily implemented and offers a suite of robust default and optional tools for SB profile extractions and related methods. The AUTOPROF pipeline is highly extensible and can be adapted for a variety of applications. The AUTOPROF code is available freely to the community at: https://github.com/ConnorStoneAstro/AutoProf.

We have compared AUTOPROF with similar widely used surface photometry codes (PHOTUTILS, XVISTA, and GALFIT) and found generally superb agreement, especially with other non-parametric solutions. However, the ease of implementation, automation, and ability to tease out faint signals in galaxy's outskirts sets AUTOPROF apart from other softwares. Indeed, it is shown that AUTOPROF, with its band averaging technique and other numerical treatments, yields SB profiles that typically reach 2–3 mag arcsec^{-2} deeper than other similar software for a given SB error. AUTOPROF is also the only method considered here which fully automates all analysis steps, making it the fastest to implement for new users.

We find that overly simplistic parametric models with only one or two components cannot adequately describe the light distribution of a galaxy, yielding larger scatter in fitted parameters than can be achieved with non-parametric approaches. Overall, AUTOPROF balances the need for complex (spatially resolved) information available in each galaxy image with the desire for fast, automated, and efficient representations of a galaxy. For large-scale applications, AUTOPROF produces reliable and extended brightness profiles. AUTOPROF is thus ideally suited for modern large-scale investigations of the detailed statistical nature of galaxy formation and evolution.

ACKNOWLEDGEMENTS

We are grateful to the Natural Sciences and Engineering Research Council of Canada, the Ontario Government, and Queen's University for support through various generous scholarships and grants. Ivo Busko, Tod Lauer, and Chien Peng have provided especially valuable comments regarding our comparisons with PHOTUTILS, XVISTA, and GALFIT; their contributions are duly acknowledged. Sean Begy, Simón Díaz García, Matt Frosst, and Mike Smith are thanked for comments that improved AUTOPROF's implementation.

DATA AVAILABILITY

The data underlying this article will be shared on reasonable request to the corresponding author(s).

REFERENCES

Akhlaghi M., 2019, preprint (arXiv:1909.11230)
Amiaux J. et al., 2012, in Clampin M. C., Fazio G. G., MacEwen H. A., Oschmann J. M., Jr, eds, SPIE Conf. Ser. Vol. 8442, Space Telescopes and Instrumentation 2012: Optical, Infrared, and Millimeter Wave. SPIE, Bellingham, p. 84420Z
Arora N., Stone C., Courteau S., Jarrett T. H., 2021, MNRAS, 505, 3135
Barden M., Häußler B., Peng C. Y., McIntosh D. H., Guo Y., 2012, MNRAS, 422, 449
Bertin E., Arnouts S., 1996, A&AS, 117, 393
Bottrell C., Torrey P., Simard L., Ellison S. L., 2017, MNRAS, 467, 2879
Bradley L. et al., 2020, Technical Report, astropy/photutils: 1.0.0. Zenodo
Burger W., Burge M., 2010, Principles of Digital Image Processing: Core Algorithms. Undergraduate Topics in Computer Science. Springer, London, Available at: https://books.google.ca/books?id = s5CBZLBakawC
Carter D., 1978, MNRAS, 182, 797
Ciambur B. C., 2015, ApJ, 810, 120
Ciambur B. C., 2016, Proc. Astron. Soc. Aust., 33, e062
Comerón S., Salo H., Knapen J. H., 2018, A&A, 610, A5
Courteau S., 1996, ApJS, 103, 363
Courteau S., Widrow L. M., McDonald M., Guhathakurta P., Gilbert K. M., Zhu Y., Beaton R. L., Majewski S. R., 2011, ApJ, 739, 20
Davis L. E., Cawson M., Davies R. L., Illingworth G., 1985, AJ, 90, 169
de Vaucouleurs G., 1948, Ann. Astrophys., 11, 247
de Vaucouleurs G., 1958, ApJ, 128, 465
Dey A. et al., 2019, AJ, 157, 168
Einasto J., 1965, Tr. Astrofiz. Inst. Alma-Ata, 5, 87
Erwin P., 2015, ApJ, 799, 226
Freeman K. C., 1970, ApJ, 160, 811
Gilhuly C., Courteau S., 2018, MNRAS, 477, 845
Hall M., Courteau S., Dutton A. A., McDonald M., Zhu Y., 2012, MNRAS, 425, 2741
Hubble E. P., 1930, ApJ, 71, 231
Ivezić Ž. et al., 2019, ApJ, 873, 111
Jedrzejewski R. I., 1987, MNRAS, 226, 747 (J87)
Kelvin L., Driver S., Robotham A., Hill D., Cameron E., 2010, in Debattista V. P., Popescu C. C., eds, AIP Conf. Ser. Vol. 1240, Hunting for the Dark: The Hidden Side of Galaxy Formation. Am. Inst. Phys., New York, p. 247
Kent S. M., 1983, ApJ, 266, 562
Kent S. M., 1985, ApJS, 59, 115
Kent S. M., Dame T. M., Fazio G., 1991, ApJ, 378, 131
Kormendy J., Bruzual A. G., 1978, ApJ, 223, L63
Lauer T. R., 1985, ApJS, 57, 473
Lauer T. R., 1986, ApJ, 311, 34
Lauer T. R. et al., 1995, AJ, 110, 2622
Lauer T. R. et al., 2005, AJ, 129, 2138
MacArthur L. A., Courteau S., Holtzman J. A., 2003, ApJ, 582, 689
McDonald M., Courteau S., Tully R. B., Roediger J., 2011, MNRAS, 414, 2055
Moffat A. F. J., 1969, A&A, 3, 455
Mosby G. et al., 2020, J. Astron. Telesc. Instrum. Syst., 6, 1
Peng C. Y., Ho L. C., Impey C. D., Rix H.-W., 2002, AJ, 124, 266
Peng C. Y., Ho L. C., Impey C. D., Rix H.-W., 2010, AJ, 139, 2097
Ratnatunga K. U., Newell E. B., 1984, AJ, 89, 176
Sérsic J. L., 1968, Atlas de Galaxias Australes. Observatorio Astronomico, Cordoba
Shai Shalev-Shwartz S. B.-D., 2014, Understanding Machine Learning: From Theory to Algorithms. Cambrige Univ. Press, Cambrige
Shannon C., 1949, Proc. IREE, 37, 10
Simard L. et al., 2002, ApJS, 142, 1
Simard L., Mendel J. T., Patton D. R., Ellison S. L., McConnachie A. W., 2011, ApJS, 196, 11
Smith M. J., Arora N., Stone C., Courteau S., Geach J. E., 2021, MNRAS, 503, 96
Stone C., Courteau S., 2019, ApJ, 882, 6
Stone C., Courteau S., Arora N., 2021, ApJ, 912, 41
Tody D., 1986, in Crawford D. L., ed., SPIE Conf. Ser. Vol. 627, Instrumentation in Astronomy VI. SPIE, Bellingham, p. 733
Tuccillo D., Huertas-Company M., Decencière E., Velasco-Forero S., Domínguez Sánchez H., Dimauro P., 2018, MNRAS, 475, 894
van der Kruit P. C., Freeman K. C., 2011, ARA&A, 49, 301
Vikram V., Wadadekar Y., Kembhavi A. K., Vijayagovindan G. V., 2010, MNRAS, 409, 1379

APPENDIX A: OTHER PHOTOMETRY METHOD COMPARISONS

This appendix provides profile comparisons between the other photometry methods for completeness. The comparisons in Fig. A1

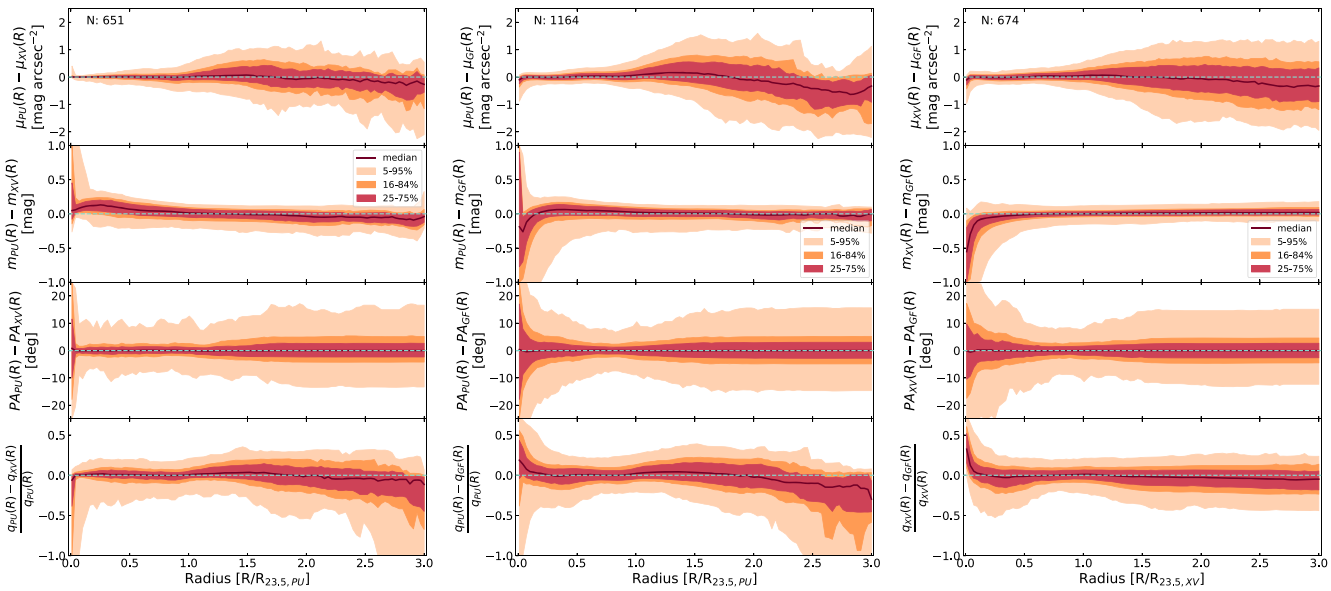

Figure A1. Comparison of radial profiles between PHOTUTILS, XVISTA, and GALFIT. Each panel formatted as in Fig. 13.

between PHOTUTILS, XVISTA, and GALFIT display near identical behaviour as reported for AUTOPROF. The consistency of these results demonstrates the reliability of AUTOPROF as a SB profile extracting algorithm. The scatter about zero can be considered as a systematic error inherent in SB profile fitting. The SB errors reported in AUTOPROF and other codes are only statistical, and can often be quite small; users should consider systematic errors of similar scale to those presented in Fig. A1 and earlier sections before establishing final SB errors.

Fig. A1(left) illustrates that SB and q for PHOTUTILS and XVISTA agree within $\sim 2R_{23.5}$ before showing a small bias (similar to findings in Section 4.1). The inner $0.1R_{23.5}$ shows again a strong discrepancy in mag, PA, and q likely due to unstable central ellipses in PHOTUTILS and simplistic bi-linear interpolation between pixels. The middle and right-hand panels in Fig. A1 show comparisons with PHOTUTILS and XVISTA against GALFIT demonstrating the same behaviour seen in Section 4.3 where there is overall agreement, though with slightly larger scatter. These figures are consistent with the description in Section 4.3 that the overly simplistic parametric models given to GALFIT cannot fully describe the complexity of late-type systems. The central axial ratio values are also larger for non-parametric analyses compared to GALFIT; this is consistent with elliptical isophotes becoming rounder towards the centre as expected in the presence of bulges and a circularizing PSF. For low resolution features on scales of the PSF, the forward modelled GALFIT solution is superior.

APPENDIX B: EXAMPLE FIT COMPARISONS

This appendix presents specific cases of profile disagreements. Fig. B1 focuses on cases of most significant disagreement in galaxy inclination (evaluated at $R_{23.5}$) between AUTOPROF and PHOTUTILS, XVISTA, or GALFIT. The first three columns show disagreement between AUTOPROF and PHOTUTILS, the middle set of three columns show disagreement between AUTOPROF and XVISTA, and the last three show disagreement between AUTOPROF and GALFIT. The galaxies in this figure represent some of the most challenging in the PROBES data set, with nearly all of them including a bar, wide spiral arms, or both. For each of the nine challenging galaxies, we show the fitted isophotes from all four methods, in several cases there are multiple methods which fail to adequately represent the galaxy.

The first column shows *VCC2070*, which has a large bar and several dust lanes through the disc. In this case, the discrepancy comes from two un-masked stars on opposite sides of the galaxy which cause PHOTUTILS to seriously missalign intermediate isophotes (only one shown) that happen to be at $R_{23.5}$ where the inclination is measured. This is a common issue for standard J87 fitting and can be circumvented with star masking or the regularization technique applied in AUTOPROF. The second column shows *UGC07524*, which has a bar-like feature and a faint, irregular, light distribution. In this case, PHOTUTILS is unable to model the light distribution beyond the bar feature and prematurely ends the light profile. AUTOPROF fails to capture the bar feature as well, but adequately finds the global light distribution. This galaxy also presented a challenge for XVISTA,

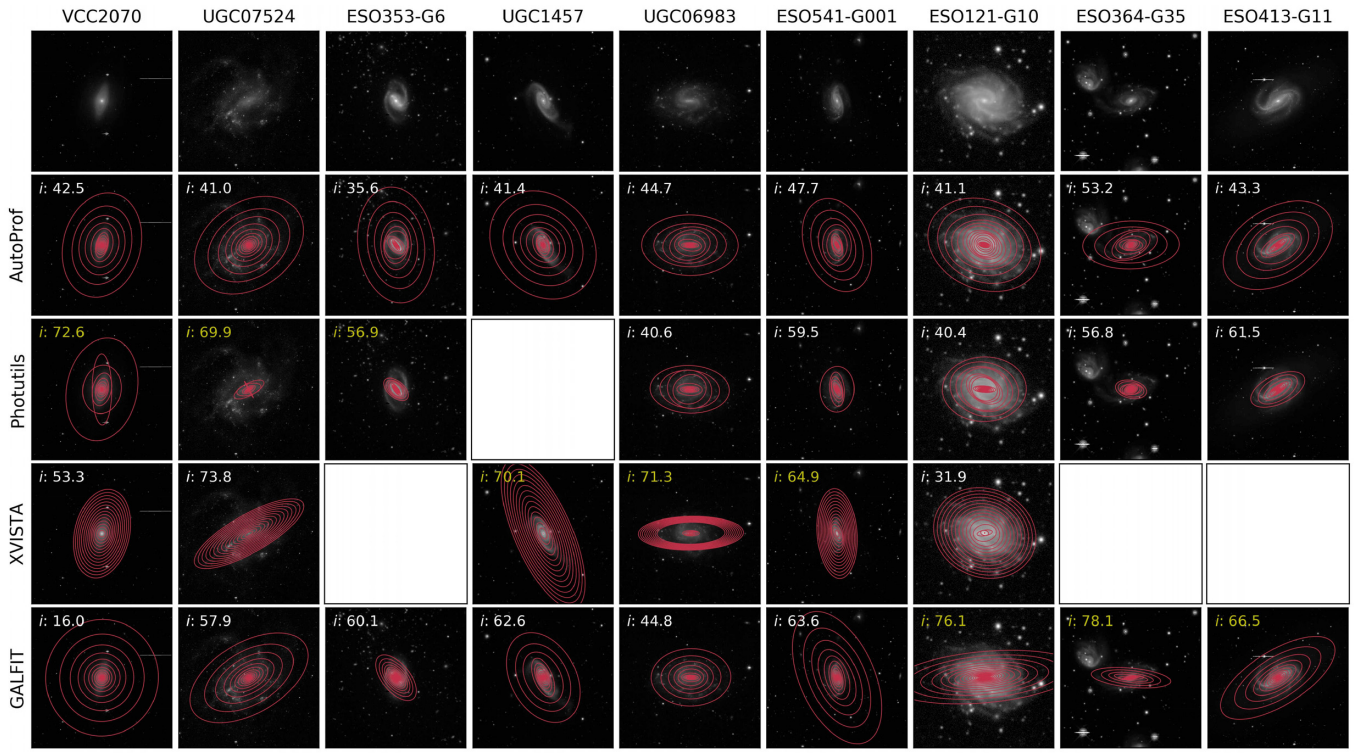

Figure B1. Comparison of most significant cases of discrepancy in inclination between AUTOPROF and the three other methods (PHOTUTILS, XVISTA, and GALFIT). The top row shows an image of a challenging galaxy with its name overhead. The second row shows AUTOPROF with its fitted ellipses overlayed. The third, fourth, and fifth rows show the fitted ellipse models for PHOTUTILS, XVISTA, and GALFIT, respectively. The first three columns are galaxies selected for greatest discrepancy with PHOTUTILS, the middle three columns are discrepancies with XVISTA, and the last the columns are discrepancies with GALFIT. The text inset gives the inclination (in degrees) from each method, with the cases of discrepancy highlighted in yellow. Figures were left empty if the given isophotal fitter could not find a solution for the galaxy.

which could only recover the bar feature, though this solution was extended to the optical edge of the galaxy. The third column shows *ESO353-G6*, a strongly barred system with a quick transition to two spiral arms and a wide opening angle. Here, both PHOTUTILS and GALFIT could only recover the bar feature, while AUTOPROF fully represented the light distribution including the sharp transition from bar to spiral arms.

The fourth column shows *UGC1457*, which has a bar-like feature at the centre and broad asymmetrical spiral arms. AUTOPROF cannot adequately fit this galaxy, and this case was not identified by the fit checks. XVISTA, however, succeeded in modelling the galaxy at all radii. PHOTUTILS failed to find a solution for this galaxy and returned no result, while GALFIT recovered the global light distribution. The fifth column shows *UGC06983*, which has a central bar and faint spiral arms. In this case, both AUTOPROF and PHOTUTILS obtained accurate models for the light distribution. XVISTA fitted only the bar feature, though the solution is extended to the optical edge of the galaxy. GALFIT (roughly) recovered the bar and accurately modelled the global light distribution using a two-component fit. The sixth column shows *ESO541-G001*, which has a bar, asymmetrical spiral arms, and a faint extended disc. Here, AUTOPROF adequately recovered all features, including the faint extended dist. XVISTA faithfully matched the main spiral structure of the galaxy, but failed to capture the faint extended disc. PHOTUTILS accurately matched the features of this galaxy, but could not extend its solution as far as AUTOPROF; GALFIT fitted the bright central structures well, but missed the faint extended disc.

The seventh column shows *ESO121-G10*, which has a bright central bar and prominent spiral arms. All methods were able to recover the central bar feature, however the GALFIT solution fails to fit the disc, causing the large discrepancy in inclination with AUTOPROF. The eighth column shows *ESO364-G35*, which has a small central bar and faint, distinct spiral features at all scales of the disc. AUTOPROF recovered the small central bar and the global structure of the galaxy while GALFIT's solution was dominated by the bright central spiral arms causing it to miss the larger disc structure. The ninth column shows *ESO413-G11*, which has a strong bar and spiral arms with a wide opening angle. Both AUTOPROF and PHOTUTILS accurately modelled the full galaxy light distribution, however GALFIT fitted only the large bar feature.

These cases of discrepancy between AUTOPROF and the other methods highlight a number of common problems encountered in elliptical isophote fitting. With the exception of *UGC1457*, AUTOPROF can handle these challenging cases in a fully automated fashion. Overall, all four methods performed satisfactorily on most galaxies. They are differentiated by their treatment of challenging cases, their spatial extent (before reaching a nominal S/N level) in the galaxy's outskirts, their execution time, and other secondary considerations.

APPENDIX C: EXAMPLE FLAGGED AUTOPROF FITS

We now present a random assortment of failed isophotal fits flagged by the *checkfit* step of the AUTOPROF pipeline (see Section 2.7). Fig. C1 presents a grid of failed fits demonstrating typical challenges that can be encountered. The most common type of failed fits are shown in Fig. C1 panels b, c, h, i, m, and n where the isophotal analysis is (inappropriately) applied to edge-on galaxies. Because edge-on galaxies do not present any aspect of their disc, surface photometry cannot and should not be attempted on those systems. AUTOPROF identifies failed fits as described in Section 2.7. Since the fit checking step is not specifically designed for edge-on galaxies,

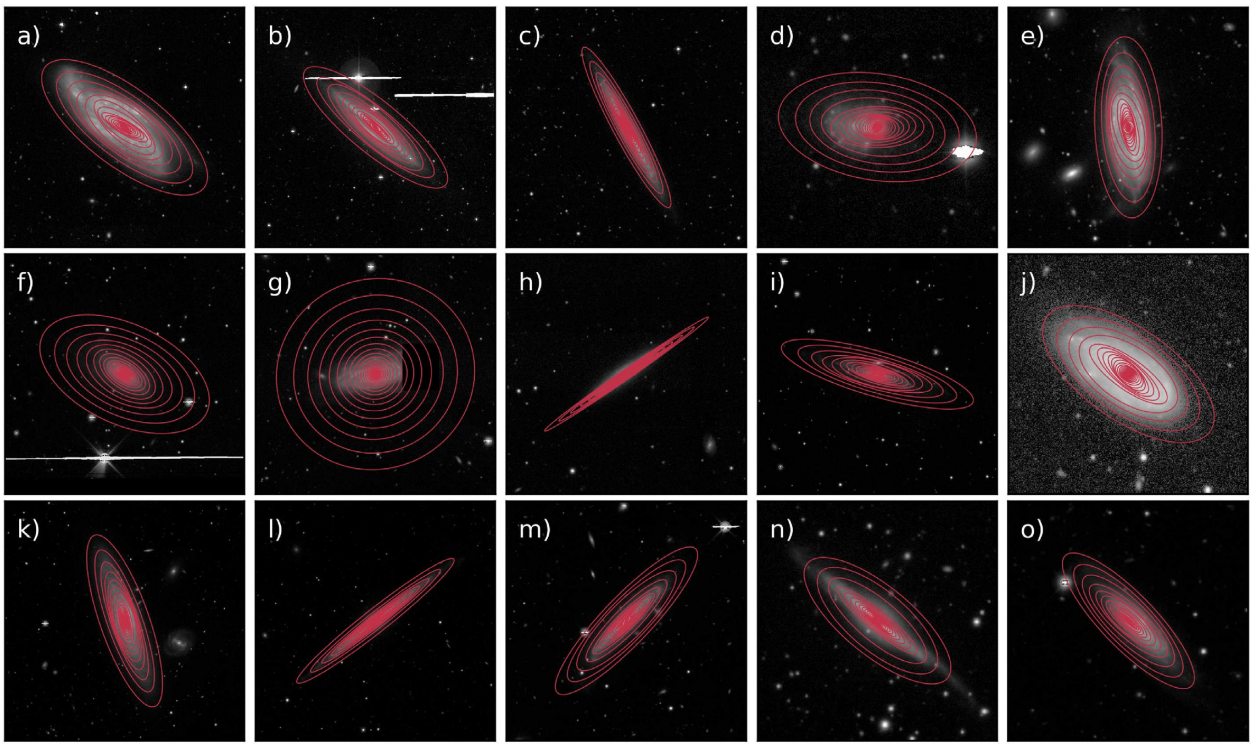

Figure C1. Cases of flagged AUTOPROF isophotal solutions as identified by the fit checks in Section 2.7. While the AUTOPROF algorithm may have converged to an optimal solution, some of these objects may simply not be adequately described by elliptical isophotes.

the user should implement their own edge-on rejection method (e.g, via radial samples or an ellipticity cut).

Fig. C1 panel d is a case where the centre finding algorithm has failed. No clear galaxy centre could be found; this is rather common for irregular galaxies and is reliably detected as a failed fit. Cases in Fig. C1 panels b, d, f, and o all have a bright interloper along (or close to) the major axis. In some cases, AUTOPROF can recover an adequate fit even though these are still flagged as potentially problematic. AUTOPROF cannot separate overlapping sources, and these cases require further attention and/or alternate analysis routines. Fig. C1 panels a, j, o, and k are examples of asymmetric galaxies. While the AUTOPROF isophotal solution follows the large scale features of these objects, elliptical isophotes should not be applied to strongly asymmetrical objects. Finally, Fig. C1 panel g is a case of the AUTOPROF optimization algorithm being trapped in a local minimum and unable to find even an approximately correct solution. The large block of missing data immediately adjacent to the galaxy is likely the culprit.

This paper has been typeset from a TEX/LATEX file prepared by the author.